Universiteit Utrecht

Editorial Board, Climate of the Past

To the editorial Board

**Faculty of Geosciences,
Department of Earth Sciences**
Marine Palynology and
Paleoceanography

Visitors Address
Vening Meineszgebouw A
Princetonlaan 8A
3584 CB Utrecht
The Netherlands

Your reference
Our reference   Manuscript to Climate of the Past
Phone   +31 30 253 9318
Fax   +31 30 253 5096
Email   p.k.bijl@uu.nl
Website   www.uu.nl/staff/pkbijl
Date   09-05-2018
Subject   Submission of manuscript to Climate of the Past

Dear Professor Thornalley, Dear editor,

Please find enclosed our final revised manuscript, entitled "**Oligocene–Miocene paleoceanography off the Wilkes Land margin (East Antarctica) based on organic-walled dinoflagellate cysts**" (cp-2017-148). Our contribution is part of a set of three companion manuscripts submitted to your journal: Hartman et al. cp-2017-153 and Salabarnada et al. CP-2017-152.

We were very pleased to see three reviewers critically assessed our submission. All three were very positive about our manuscript, and raised some critical points of discussion and suggestions. We used these reviews to revise our manuscript accordingly, which results in a much clearer and better structured presentation of our results and interpretation.

Specifically, we adjusted the comparison of our dinocyst assemblage data with lithologic interpretations made in the companion paper Salabarnada et al. who in their revision added detailed lithologic descriptions for the Miocene part of the succession. This enabled us to extend our lithology-dinocyst assemblage comparison into the Miocene, as was specifically suggested by two of the reviewers. This makes our exercise much clearer to the reader, while reinforcing the conclusions made in our first submission, notably that we see profound differences in dinocyst assemblages in independently interpreted interglacial sediments compared to glacial sediments, reflecting profound ice-proximal oceanographic changes associated to astronomically-paced glacial-interglacial changes.

We also added a section reviewing the evidence for *Selenopemphix antarctica* as indicator for sea-ice conditions, as was specifically suggested by reviewer 2.

The final version of the manuscript contains 7 figures, 2 tables and about 6500 words.

In anticipation of your reply,

Best regards, also on behalf of my co-authors,

Peter K. Bijl
Corresponding author

1 **Oligocene–Miocene paleoceanography off the Wilkes Land margin**

2 **(East Antarctica) based on organic-walled dinoflagellate cysts**

4 Peter K. Bijl[1]*, Alexander J. P. Houben[2], Julian D. Hartman[1], Jörg Pross[3], Ariadna

5 Salabarnada[4], Carlota Escutia[4], Francesca Sangiorgi[1]

7 1 Marine Palynology and Paleoceanography, Laboratory of Palaeobotany and

8 Palynology, Department of Earth Sciences, Faculty of Geosciences, Utrecht University.

9 P.O. Box 80.115, 3508 TC Utrecht, The Netherlands

11 2 Geological Survey of the Netherlands, Netherlands Organisation for Applied

12 Scientific Research (TNO), Princetonlaan 6, 3584 CB, Utrecht, The Netherlands

14 3 Paleoenvironmental Dynamics Group, Institute of Earth Sciences, Heidelberg

15 University, Im Neuenheimer Feld 234, 69120 Heidelberg, Germany

17 4 Instituto Andaluz de Ciencias de la Tierra, CSIC-UGR, 18100 Armilla, Spain

19 * to whom correspondence should be addressed.

20 Email: p.k.bijl@uu.nl; phone +31 30 253 9318

Abstract

Next to atmospheric CO_2 concentrations, ice-proximal oceanographic conditions are a critical factor for the stability of Antarctic marine-terminating ice sheets. The Oligocene and Miocene epochs (~34–5 Ma ago) were time intervals with atmospheric CO_2 concentrations between those of present-day and those expected for the near future. As such, these past analogues may provide insights into ice-sheet volume stability under warmer-than-present-day climates. We present organic-walled dinoflagellate cyst (dinocyst) assemblages from chronostratigraphically well-constrained Oligocene to mid-Miocene sediments from Integrated Ocean Drilling Program Expedition (IODP) Site U1356. Situated offshore the Wilkes Land continental margin, East Antarctica, the sediments from Site U1356 have archived the dynamics of an ice sheet that is today mostly grounded below sea level. We interpret dinocyst assemblages in terms of paleoceanographic change on different time scales, i.e., with regard to both glacial-interglacial and long-term variability. Our record shows that a sea-ice related dinocyst species, *Selenopemphix antarctica*, occurs only for the first 1.5 Ma of the early Oligocene, following the onset of full continental glaciation on Antarctica, and after the mid-Miocene Climatic Optimum. Dinocysts suggest a weaker-than-modern sea-ice season for the remainder of the Oligocene and Miocene. The assemblages generally bear strong similarity to present-day open-ocean, high-nutrient settings north of the sea-ice edge, with episodic dominance of temperate species similar to those found in the present-day subtropical front. Oligotrophic and temperate surface waters prevailed over the site notably during interglacial times, suggesting that

46   **the positions of the (subpolar) oceanic frontal systems have varied in**

47   **concordance with Oligocene-Miocene glacial-interglacial climate variability.**

48

49   **1. Introduction**

50   The proportion of the East Antarctic ice sheet that is presently grounded below sea

51   level is much larger than originally interpreted (Fretwell et al., 2013). This implies

52   that a larger part of the continental ice sheet is sensitive to basal melting by warm

53   waters than previously thought (Shepherd et al., 2012; Rignot et al., 2013; Wouters et

54   al., 2015), and that a higher amplitude and faster rate of sea-level rise is to be

55   expected under future climate warming than previously acknowledged (IPCC, 2013).

56   Studying the amount and variability of Antarctic ice volume in periods with high

57   atmospheric CO_2 concentrations ($p$$CO_2$) provides additional insight into ice/ocean

58   feedback processes. Foster and Rohling (2013) compared sea-level and atmospheric

59 $p$$CO_2$ concentrations on geological timescales. Their study suggests that global ice

60   sheets were rather insensitive to climate change when atmospheric $p$$CO_2$ ranged

61   between 400 and 650 parts per million in volume (ppmv). During the Oligocene and

62   Miocene, atmospheric $p$$CO_2$ ranged between 400 and 650 ppmv (Foster et al., 2012;

63   Badger et al., 2013; Greenop et al., 2014). Crucially, similar $p$$CO_2$ levels are expected

64   for the near future given unabated carbon emissions (IPCC, 2013), implying that

65   global ice volume may not change much under these $p$$CO_2$ scenarios.

66   In contrast to the invariant global ice volume inferred by Foster and Rohling

67   (2013), a strong (up to 1 per mille; ‰) variability is preserved in deep-sea benthic

68   foraminiferal oxygen isotope (hereafter benthic $\delta^{18}O$) data (Pälike et al., 2006;

69   Beddow et al., 2016; Holbourn et al., 2007; Liebrand et al., 2011; 2017). These

70   benthic $\delta^{18}O$ data reflect changes in continental ice volume (primarily on Antarctica)

71   and deep-sea temperature. The latter is strongly coupled to polar surface-water

72   temperature, as deep-water formation was predominantly at high latitudes at that

73   time (Herold et al., 2011). High-amplitude variations in benthic $\delta^{18}O$ thus suggest

74   either (i) strong climate dynamics in the high latitudes with relatively minor ice-

75   volume change (which would be in accordance with numerical modelling

76   experiments (Barker et al., 1999) and the interpretation of Foster and Rohling

77   (2013)), or (ii) strong fluctuations in Antarctic ice volume, with relatively subdued

78   temperature variability (which would be in accordance with indications for unstable

79   Antarctic ice sheets under warmer-than-present climates (Cook et al., 2013; Greenop

80   et al., 2014; Rovere et al., 2014; Sangiorgi et al., 2018). If one assumes a present-day

81    $\delta^{18}O$ composition (-42‰ *versus* standard mean ocean water (SMOW)) for Oligocene–

82   Miocene Antarctic ice-sheets and modern deep-water temperature (2.5°C), the

83   benthic $\delta^{18}O$ fluctuations during the Oligocene–Miocene suggest long-term ice-sheet

84   variability to have fluctuated considerably (Liebrand et al., 2017). Similarly strong

85   fluctuations were observed in sedimentary records from the Gippsland Basin,

86   southeast Australia (Gallagher et al., 2013). Meanwhile, deep-sea temperatures have

87   fluctuated considerably as well during the Oligocene and Miocene (Lear et al., 2004),

88   which is further evident from ice-free geologic episodes (Zachos et al., 2008).

89   Therefore, a combination of deep-sea temperature and ice-volume changes is likely

90   represented in these records. Further ice-proximal reconstructions of climate, ice-

91   sheet and oceanographic conditions are required to provide an independent

92   assessment of the stability of ice sheets under these higher-than present-day pCO$_2$

93   concentrations.

94   While Oligocene–Miocene climates may bear analogy to our future in terms of

95   pCO$_2$ concentrations, the uncertainties and differences in Antarctic paleotopography

96   must be considered in any such comparison, as this factor critically determines the

97   proportion of marine-based *versus* land-based ice. An Antarctic continent with low

98   topography would result in more ice sheets being potentially sensitive to basal melt

99   and as such a higher sensitivity of these ice sheets to climate change. Moreover, the

100   fundamentally different paleogeographic configuration of the Southern Ocean during

101   that time as compared to today should also be considered (Figure 1). The

102   development and strength of the Antarctic Circumpolar Current (ACC) connecting the

103   Atlantic, Indian and Pacific Ocean basins (Barker and Thomas, 2004; Olbers et al.,

104   2004) depend on the basin configuration (i.e., the width and depth of the gateways as

105   well as the position of the landmasses). The exact timing when the ACC reached its

106   modern-day strength is still uncertain, ranging from the middle Eocene (41 Ma) to as

107   young as Miocene (23 Ma; Scher and Martin, 2004; Hill et al., 2013; Scher et al., 2015).

108   Whether and, if so, how the development of the ACC has influenced latitudinal heat

109   transport, ice-ocean interactions and the stability of Antarctic continental ice has

110   remained poorly understood.

111   To directly assess the role of ice-proximal oceanography on ice-sheet stability

112   during the Oligocene–Miocene, ice-proximal proxy-records are required. Several

113   ocean drilling expeditions have been undertaken in the past to provide insight in the

114   history of the Antarctic ice sheets (Barrett, 1989; Wise and Schlich, 1992; Barker et

115   al., 1998; Robert et al., 1998; Wilson et al., 2000; Cooper and O'Brien, 2004; Exon et

116   al., 2004; Harwood et al., 2006; Escutia and Brinkhuis, 2014). For some of the

117   retrieved sedimentary archives, age control was particularly challenging due to the

118 paucity of useful means to calibrate them to the international time scale. As a

119 consequence, the full use of these archives for the generation of paleoceanographic

120 proxy records and ice-sheet reconstructions has remained limited.

121   In 2010, Integrated Ocean Drilling Program (IODP) Expedition 318 drilled an

122 inshore-to-offshore transect off Wilkes Land (Fig. 1a), a sector of East Antarctica that

123 is interpreted to be highly sensitive to continental ice-sheet melt (Escutia et al.,

124 2011). The sediments recovered from IODP Site U1356 are from the continental rise

125 of this margin (Escutia et al., 2011) and hence contain a mixture of shelf-derived

126 material and pelagic sedimentation. Dinocyst events in this record have been recently

127 tied to the international time scale through integration with calcareous nannofossil,

128 diatom and magnetostratigraphic data (Bijl et al., 2018). By Southern Ocean

129 standards, the resulting stratigraphic age frame for the Oligocene–Miocene record of

130 Site U1356 (Fig. 2; Table 1) is of high resolution. In this paper, we investigate the

131 dinocyst assemblages from this succession by utilizing the strong relationships

132 between dinocyst assemblage composition and surface-water conditions of today's

133 Southern Ocean (Prebble et al., 2013). We reconstruct the oceanographic regimes

134 during the Oligocene and mid-Miocene, and evaluate their implications. We further

135 compare the palynological data with lithological observations and their

136 interpretations from Salabarnada et al. (submitted, this volume). Pairing the

137 sedimentological interpretations and biomarker-derived absolute sea-surface

138 temperature (SST) reconstructions from Site U1356 (Hartman et al., submitted, this

139 volume) with our dinocyst assemblage data, we reconstruct the paleooceanographic

140 conditions off Wilkes Land and assess their variability both on glacial-interglacial and

141 longer-term times scales.

142

2. Material

       2.1 Site description for IODP Hole U1356A

Samples were taken from IODP Hole U1356A, the only hole from Site U1356, cored on

the continental rise of the Wilkes Land margin, East Antarctica (Figure 1a; present

coordinates 63°18.6' S, 135°59.9' E; Escutia et al., 2011). The paleolatitude calculator

of van Hinsbergen et al. (2015) was used to reconstruct the paleolatitudinal history of

the site (Figure 1, between -59.8±4.8°S and -61.5±3.3° S between 34 Ma and 13 Ma,

respectively). Hole U1356A reaches a depth of 1006.4 m into the seabed (Escutia et

al., 2011). Oligocene to upper Miocene sediments were recovered between 890 and 3

mbsf (meters below sea floor, Figure 2; Tauxe et al., 2012; revised according to Bijl et

al., 2018). The uppermost 95 meters of the hole were poorly recovered; sediments

consisted of unconsolidated mud strongly disturbed by rotary drilling (Escutia et al.,

2011). Hence, we focused our investigation on the interval between Cores 11R to 95R

Section 3 (95.4–894 mbsf; 10.8–33.6 Ma; Figure 2).

       2.2 Lithology in IODP Hole U1356A

In the interval between 95.4 and 894 mbsf, nine lithologic units have been recognized

during shipboard analysis (Figure 2; Escutia et al., 2011). Salabarnada et al.

(submitted, this volume) present a detailed lithologic column of the Oligocene and

Miocene sediments. The lithologic facies described in Salabarnada et al. (submitted,

this volume) will help us compare paleoceanographic differences between climatic

extremes. Salabarnada et al. (submitted this volume) distinguished various lithologies

along with interpretations of their depositional settings which can be summarized as:

166   1) laminated silty clay sediments (interpreted as glacial deposits; hereafter Fg), 2)

167   bioturbated siltstones and claystones that in some intervals are carbonate-cemented

168   (interpreted as interglacial deposits, hereafter Fi), and 3) perturbed mass transport

169   deposits (MTDs): slumps and debris flows. We refer to Salabarnada et al. (submitted

170   this volume; Fig S2) for a detailed description of these facies, and to the

171   supplementary datasets on pangaea for more detailed separation of our palynological

172   results per facies type.

173

174   2.3 Bio-magnetostratigraphic age model for IODP Hole U1356A

175   Stratigraphic constraints for the Oligocene–Miocene succession from IODP Hole

176   U1356A are provided through calcareous nannoplankton, radiolarian, diatom and

177   sparse palynological biostratigraphy, complemented by magnetostratigraphy (Tauxe

178   et al., 2012). Bijl et al. (2018) and Crampton et al. (2016) have updated the existing

179   age model for Site U1356 for the Oligocene and Miocene parts of the succession,

180   respectively. In their efforts, they recalibrated the tie points to the international time

181   scale of Gradstein et al. (2012). We here follow their revision of the age model (Table

182   1). We infer ages by linear interpolation between tie points (Figure 2; Table 1).

183

184   2.4 Depositional setting at IODP Site U1356

185   The depositional setting at Site U1356 changed from a shallow mid-continental shelf

186   in the early Eocene (Bijl et al., 2013a) to a deep continental rise environment by the

187   Oligocene (Houben et al., 2013) due to subsidence of the Wilkes Land margin (e.g.,

188   Close et al., 2009). Regional correlation of the facies at Hole U1356A via seismic

189   profiles suggests a mix of distal-submarine fan and hemipelagic sedimentation during

190 the early Oligocene, grading into channel-levee deposits in the later Oligocene

191 (Escutia et al., 2011). The boundary between these two different depositional settings

192 is at ~650 mbsf; there, sedimentation rates increase, and the documentation of mass-

193 transport deposits from this depth upwards suggests shelf-derived erosion events on

194 the Wilkes Land continental slope (Escutia et al., 2011).

195

196 **3. Methods**

197   3.1 Palynological sample processing

198 The sample processing and analytical protocols as followed in this study are in

199 accordance with standard procedures and have been previously described by Bijl et

200 al. (2013b; 2018). The 25 species of dinocysts new to science, which are formally (2

201 species) and informally (23 species) described in Bijl et al. (2018), fit into known and

202 extant genera, and therefore could be confidently included in the ecological groups as

203 described below. We refer to Bijl et al. (2018) for an extensive overview (including

204 plates) of the dinocyst species encountered.

205

206   3.2 Ecological grouping of dinocyst taxa

207 Bijl et al. (2018) provided additional statistical evidence to distinguish in situ

208 dinocysts from those that are reworked from older strata. In this paper, we follow the

209 interpretations of Bijl et al. (2018) and divide the dinocyst species into a reworked

210 and an in situ group (Table 2). To use the in situ dinocyst assemblages for

211 oceanographic reconstructions, we rely on the observation that many taxa in the

212 fossil assemblages have morphologically closely related modern counterparts. This

213 approach takes advantage of studies on the present-day relationship between

Southern Ocean microplankton in general and dinoflagellate cysts in particular and their surface-water characteristics (e.g., Eynaud et al., 1999; Esper and Zonneveld, 2002, 2007; Prebble et al., 2013). We assign Oligocene–Miocene dinocyst taxa to present-day eco-groups interpreted from the clusters identified by Prebble et al. (2013), which appear to be closely related to the oceanic frontal systems in the Southern Ocean (Figure 3). Supporting evidence for the ecologic affinities of the dinocyst groups comes from empirical data, such as correlation of abundances with other sediment properties or proxies (Sluijs et al., 2005; Egger et al., 2018), for instance with regard to the affinities of *Nematosphaeropsis labyrinthus*, *Operculodinium* spp., *Pyxidinopsis* cpx. (this includes *Corrudinium* spp. and *Cerebrocysta* spp.) and *Impagidinium* spp. There is further abundant evidence, both empirically (e.g., Sluijs et al., 2003; Houben et al., 2013) and from modern observations (Zonneveld et al., 2013; Prebble et al., 2013; Eynaud et al., 1999), that links the abundance of protoperidinioid dinocysts to high surface-water productivity. The arguably most important inference from the surface-sediment sample study of Prebble et al. (2013) is that *Selenopemphix antarctica* is common to dominant (10–90%) south of the Antarctic polar front (AAPF). In particular, the Antarctic continental shelf exhibits a consistently high relative abundance of *Selenopemphix antarctica*. In addition to the surface samples of Prebble et al. (2013), this is also evident at the Wilkes Land margin proper (IODP Site U1357; Hartman, Bijl and Sangiorgi, pers. obs.), at Prydz Bay (Storkey, 2006), in the Weddell (Harland and Pudsey, 1999) and Ross Seas (Hartman, Bijl and Sangiorgi, pers. obs), and in the southern Indian Ocean (Marret and de Vernal, 1997): samples all contain very abundant to dominant (>50 to 90%) *S. antarctica*. The dominance of this species

238   becomes even stronger when considering that assemblages in these surface samples

239   often include cysts that are not easily preserved in older sediments such as that of

240   *Polarella glacialis*. Leaving these dinocyst out of the dinocyst sum increases the

241   relative abundance of *Selenopemphix antarctica* in surface samples. Notably, surface-

242   sediment samples outside of the AAPF never have dominant (~90%) *Selenopemphix*

243   *antarctica* (Prebble et al., 2013). Another important observation is that the surface-

244   sediment samples south of the AAPF are generally devoid of gonyaulacean dinocysts,

245   with the exception of two species of *Impagidinium* (i.e., *I. pallidum* and *I. sphaericum*)

246   that may occur, although neither abundantly (Prebble et al., 2013) nor exclusively

247   (e.g., Zevenboom, 1995; Zonneveld et al., 2013), in ice-proximal locations. Abundant

248   *Nematosphaeropsis labyrinthus* occurs exclusively in regions outside of the

249   Subantarctic Front, and particularly near the Subtropical Front. Thus, we conclude

250   from the available literature a dominance of *S. antarctica* south of the AAPF, a

251   dominance of other protoperidinioid dinocysts at and north of the AAPF, mixed

252   protoperidinioid and gonyaulacoid dinocysts (with a notable occurrence of

253   *Nematosphaeropsis labyrinthus* at the sub-Antarctic front (SAF), and mixed

254   gonyaulacoid dinocysts at and outside of the subtropical front (STF). These trends

255   represent a north-south transition from sea-ice-influenced to cold upwelling/high

256   nutrient to warm-temperate/lower nutrient conditions, respectively. We use these

257   affinities to reconstruct past oceanographic conditions at the Wilkes Land continental

258   margin.

259

260   **4. Results**

261   4.1 Palynological groups

262   In our palynological analysis we separated palynomorph groups into four categories:

263   reworked dinocysts (following Bijl et al. (2018); Table 2), in situ dinocysts, acritarchs,

264   and terrestrial palynomorphs. Our palynological slides further contain a varying

265   amount of pyritized diatoms and a minor component of amorphous organic matter,

266   which is not further considered in this study. The relative and absolute abundances of

267   the four palynomorph groups vary considerably throughout the studied interval

268   (Figure 4). Reworked dinocysts are ubiquitous throughout the record, and are

269   particularly abundant in the lowermost 40 meters of the Oligocene and in the Upper

270   Oligocene. In situ dinocysts dominate mid-Oligocene and mid-Miocene palynomorph

271   assemblages. Chorate, sphaeromorph and *Cymatiosphaera*-like acritarchs (which are

272   not further taxonomically subdivided) dominate the assemblage in the Upper

273   Oligocene and into the mid-Miocene, while terrestrial palynomorphs (which are

274   considered in situ and not reworked from older strata (Strother et al., 2017)) are a

275   constant minor (a few % of the total palynomorph assemblage) component of the

276   total palynomorph assemblage (Fig. 4). The terrestrial palynomorphs and the

277   paleoclimatic and paleoecological interpretations derived from them will be

278   presented in another study.

279

280   4.2 In situ dinocyst assemblages

281   Throughout the Oligocene, in situ dinocyst assemblages are dominated by

282   protoperidinioid dinocysts, notably *Brigantedinium* spp., *Lejeunecysta* spp., *Malvinia*

283   *escutiana,* and *Selenopemphix* spp. (Figure 4), all of which are cysts of heterotrophic

284   dinoflagellates (e.g., Esper and Zonneveld, 2007). Among these protoperidinioid

285   cysts, *S. antarctica* is frequently present (up to 39% of the in situ assemblage), but

286   only between 33.6 and 32.1 Ma (earliest Oligocene) and after 14.2 Ma (i.e., during and

287   after the mid-Miocene climatic transition; Fig. 5). The remainder of the record is

288   almost entirely devoid of *S. antarctica*. This is much in contrast to the dinocyst

289   assemblages nearby Site U1356 today, which are dominated by this taxon (Prebble et

290   al., 2013). Instead of *S. antarctica*, other protoperidinioid dinocysts dominate during

291   the Oligocene and Miocene, such as *Brigantedinium* spp., several *Lejeunecysta* species

292   and *Selenopemphix nephroides*, which have close affinities to high-nutrient conditions

293   in general (e.g., Harland et al., 1999; Zonneveld et al., 2013), but are not specifically

294   restricted to sea-ice-proximity or the Southern Ocean. Today, these three genera

295   dominate dinocyst assemblages in high-nutrient settings at or outside of the AAPF

296   (Prebble et al., 2013). A varying abundance of protoperidinioid dinocysts could not be

297   placed with confidence into established protoperidinioid dinocyst genera. These are

298   grouped under 'protoperidinioid spp. pars' (Figure 4; Bijl et al., 2018) and are here

299   assumed to exhibit the same heterotrophic life-style as the other protoperidinioid

300   dinocyst genera.

301   Next to protoperidinioid dinocysts, gonyaulacoid dinocysts also occur in relatively

302   high abundances throughout the record from Site U1356. They comprise both known

303   and previously unknown (Bijl et al., 2018) species of *Batiacashaera, Pyxidinopsis,*

304   *Corrudinium, Cerebrocysta, Nematosphaeropsis, Impagidinium, Operculodinium*, and

305   *Spiniferites* (Fig. 4; 5). The 'others' group represents exclusively gonyaulacoid species

306   such as *Invertocysta tabulata* and *Gelatia inflata*. Except for the extinct genera

307   *Batiacasphaera* and *Cerebrocysta* and some genera in the 'others' group, all the other

308   genera are still extant and represent phototrophic dinoflagellates (Zonneveld et al.,

309   2013). Their abundance is at the expense of the assumed heterotrophic

310   protoperidinioid dinocysts. A marked increase in abundance of gonyaulacoid cysts is

311   associated with the mid-Miocene Climate Optimum (MMCO between ~17 and 15 Ma;

312   Fig. 4, 5; Sangiorgi et al., 2018). Of the gonyaulacoid taxa, *Nematosphaeropsis*

313   *labyrinthus* is associated with frontal systems of the present-day Southern Ocean

314   (Prebble et al., 2013) and of the North Atlantic Ocean (Boessenkool et al., 2001;

315   Zonneveld et al., 2013).

316

317   4.3 Comparison between palynological data and lithological facies

318   The Oligocene-Miocene sediments from Site U1356 comprise distinctive alternations

319   of lithologic facies throughout the section (Salabarnada et al., submitted, this volume;

320   Figure S2). Laminated (Fg) and bioturbated sediments, that are in some intervals are

321   carbonate-rich (Fi) alternate on orbital time scales and this pattern is in some

322   intervals disrupted by slumps and/or debris flows. We here evaluate and compare

323   the palynological content of each of these facies both in terms of absolute and relative

324   abundance of the main palynomorph groups: reworked dinocysts, in situ dinocysts,

325   acritarchs and terrestrial palynomorphs, and relative abundance of in situ dinocyst

326   eco-groups.

327

328   4.3.1 Palynomorph groups and lithology

329   There are distinct differences in the relative and absolute abundances of the

330   palynomorph groups between the different lithologies (Figure 6). The highest relative

331   and absolute abundances of reworked dinocysts occur in the slump and Fi facies (Fig.

332   6), particularly those of early Oligocene age (EOT slumps and bioturbated siltstones

333   in Supplementary datasets), in line with observations of Houben et al. (2013).

334   Reworking is a minor component of the palynomorph assemblage in the other

335   lithologies for most samples, with a higher absolute abundance in Fi deposits than in

336   glacial deposits. This suggests that submarine erosion of Eocene continental shelf

337   material was particularly prominent during interglacial times, when arguably sea

338   level along the Wilkes Land margin was lower (Stocchi et al., 2013). The relative and

339   absolute abundance of *in-situ* dinocysts is highest in the interglacial and glacial

340   deposits and the slumps (Figure 6). Acritarchs reach highest relative and absolute

341   abundances in Fi facies and in the debris flows (Figure 6). Terrestrial palynomorphs

342   are most abundant in the lower Oligocene slumps and Fi sediments (Supplementary

343   tables) but have low relative abundance in all lithologies (Figure 6).

344

345   4.3.2 In situ dinocyst eco-groups and their abundance per facies

346   The in situ dinocyst eco-groups are also compared with the lithological facies (Figure

347   7). The Fg glacial facies contains generally more peridinioid (heterotrophic)

348   dinocysts, while the Fi interglacial facies contains more gonyaulacoid (oligotrophic)

349   dinocysts, but more information is to be seen when focussing on the individual eco-

350   groups. The abundance of *Selenopemphix antarctica* is low throughout the record (0–

351   5%), with the exception of the interval post-dating the MMCO and the lowermost

352   Oligocene, where the taxon reaches occasionally more than 20% (Figs. 4, 5). *S.*

353   *antarctica* reaches highest abundances in the slump facies and Fg and is less

354   abundant in the other lithologies (Figure 7). *Selenopemphix* spp. reaches highest

355   relative abundances in the Fg facies. *Lejeunecysta* spp. and *Protoperidinium* spp. pars.

356   show no noticeable variance in relative abundance in any of the lithologies.

357   *Brigantedinium* spp. is clearly higher abundant in the Fg facies than in the Fi facies.

358 *Malvinia escutiana* abundances seem to be higher in Fi than in Fg (Figure 7), although

359 this species has a stratigraphic occurrence that is limited to the early Oligocene (Bijl

360 et al., 2018). *Nematosphaeropsis labyrinthus*, *Pyxidinopsis* cpx, *Operculodinium* spp.,

361 and *Impagidinium* spp. reach higher relative abundances in Fi than in Fg facies,

362 whereas the abundance of *Batiacasphaera* spp. seems invariant to facies.

363

364 **5. Discussion**

365  5.1 Paleoceanographic interpretation of the dinocyst assemblages

366 The composition of the dinoflagellate cyst assemblages in the Wilkes Land record

367 reflect changes in surface-ocean nutrients, sea- surface temperature conditions and

368 paleoceanographic features. We will discuss these implications in the following.

369

370  5.1.1 Surface-ocean nutrient conditions

371 The general dominance of heterotrophic dinocysts in the Oligocene–Miocene

372 assemblages indicates overall high nutrient levels in the surface waters. Given the

373 offshore geographic setting, we therefore infer that surface waters at Site U1356

374 experienced upwelling associated to the AAPF during most of the Oligocene and

375 Miocene. We can exclude the possibility that nutrients were brought to the site via

376 river runoff given the anticipated small catchment area that experienced liquid

377 precipitation in the Wilkes Land hinterland, the low amounts of terrestrially-derived

378 (amorphous) organic matter in the palynological residues and relatively low

379 branched over isoprenoid tetraether (BIT) index values (Hartman et al., submitted

380 this volume) that indicates predominantly marine organic matter. The exception may

381   be the mid-Miocene climatic Optimum (Sangiorgi et al., 2018) when considerable soil-

382   derived organic matter reached the site.

383   The occasionally abundant gonyaulacoid cyst taxa encountered in our record

384   suggest that at times surface waters were much less nutrient-rich supported the

385   growth of oligotrophic dinoflagellates. Notably, these taxa are typical for outer-shelf

386   to oceanic or outer neritic settings (e.g., Sluijs et al., 2005; Zonneveld et al., 2013;

387   Prebble et al., 2013), which makes it unlikely that they were reworked from the

388   continental shelf. Indeed, they show low relative abundances in the perturbed

389   deposits (Figure 7). Although the members of these genera have relatively long

390   stratigraphic ranges extending back into the Eocene, most of the species encountered

391   at Site U1356 are not present in Eocene continental shelf sediments in the region

392   (e.g., Wrenn and Hart, 1988; Levy and Harwood, 2000; Brinkhuis et al., 2003a, b; Bijl

393   et al., 2011; 2013a, b). This makes it unlikely that they are reworked from Eocene

394   strata. In addition, statistical analysis also yields that these species are part of the in

395   situ assemblage (Bijl et al., 2018). These different lines of evidence lead us to

396   interpret them as part of the in situ pelagic assemblage in our study, which allows us

397   to interpret their paleoceanographic implications based on their modern affinities.

398   The absence of these taxa in modern surface waters south of the AAPF is probably

399   caused by a combination of different factors: It can be connected to low sea-surface

400   temperatures and an isolation by strong eastward currents, but also the abundance

401   and seasonally concentrated availability of nutrients, all of which make the proximal

402   surface waters off Antarctica a highly specialistic niche unfavourable for these

403   species. Apparently, surface-water conditions during the Oligocene and Miocene were

404   such that these oligotrophic species could at times proliferate so close to the Antarctic

405   margin.

406

407   5.1.2 Sea-surface temperature

408   The best modern analogues for the dinocyst assemblages in our record are to be

409   sought off the southern margins of New Zealand and Tasmania (as inferred from

410   Prebble et al., 2013; Figure 2). Today, these regions feature a mix between

411   protoperidinioid dinocysts along with gonyaulacoid dinocyst genera such as

412   *Nematosphaeropsis*, *Operculodinium* and *Impagidinium*. These assemblages prevail in

413   surface waters with mean annual temperatures of 8–17°C (Prebble et al., 2013) and

414   therefore suggest relatively warm surface water temperatures close to the Wilkes

415   Land margin. In support of this, a bayesian approach on the TEX_{86} index values at Site

416   U1356 (presented in Sangiorgi et al., 2018; Hartman et al., submitted, this volume)

417   also suggests the Southern Ocean mid-latitudes as a modern-analogue region and

418   reconstructs a paleotemperature range of 8–20°C for the Oligocene–Miocene at Site

419   U1356, with values in excess of 24°C for the late Oligocene (Hartman et al., submitted,

420   this volume). Futher, supporting evidence for temperate Oligocene–Miocene surface

421   waters comes from the abundance of nannofossils encountered in the sediments

422   (Escutia et al., 2011; Salabarnada et al., submitted this volume). Today, carbonate-

423   producing plankton is rare in high-latitude surface waters south of the AAPF (Eynaud

424   et al., 1999). Moreover, the remains of the few pelagic carbonate-producing

425   organisms living at high latitudes rarely reach the ocean floor because of strong

426   upwelling of relatively CO_2-rich, corrosive waters (e.g., Olbers et al., 2004). Hence, the

427   presence of carbonate-rich intervals during the Oligocene–Miocene at Site U1356

428 along with the encountered oligotrophic, temperate dinocysts suggests

429 fundamentally warmer surface-water conditions than today.

430

431   5.1.3 Surface paleoceanography

432 The strong similarity of Oligocene–Miocene dinocyst assemblages at Site U1356 with

433 those today occurring much further north (i.e.., around Tasmania and Southern New

434 Zealand (Prebble et al., 2013) suggests a fundamentally different *modus operandi* of

435 Southern Ocean surface oceanography. The strict latitudinal separation of dinocyst

436 assemblages in the Southern Ocean today (Prebble et al., 2013) is likely due to

437 different surface water masses present across the oceanic fronts where strong wind-

438 driven divergence around 60° S (known as the Antarctic Divergence; e.g., Olbers et al.,

439 2004), strong sea-ice season and/or the vigorous Antarctic Circumpolar Current are

440 in place. The strength and position of the AAPF during the Oligocene–Miocene is not

441 well understood. Climate model (GCM) experiments under Miocene boundary

442 conditions suggest that west and east wind drifts prevailed south and north of 60°S,

443 respectively (Herold et al., 2011). This wind orientation determined the average

444 position of the Antarctic Divergence at 60°S during the Oligocene and Miocene,

445 similar to today. This suggests that Site U1356 was likely directly overlain by the

446 AAPF. However, the significantly warmer, more oligotrophic dinocyst assemblages off

447 Wilkes Land throughout the Oligocene–Miocene argue against proximity to the AAPF.

448 The position of the AAPF relative to that of Site U1356 strongly determines the

449 likelihood of southward transport of low-latitude waters towards the site. A

450 southward position of the AAPF relative to Site U1356 would greatly enhance the

451 possibility for a southward migration of temperate surface water masses towards the

452   site. A northward position of the AAPF relative to the site would make such a

453   latitudinal migration much more difficult. The presence of carbonate in these deep

454   marine sediments also suggests that upwelling of corrosive waters through the

455   (proto-)Antarctic Divergence was either much reduced or located elsewhere.

456   Therefore, we deduce that the occurrence of the oligotrophic, temperate dinocysts is

457   an evidence for a southward position of the AAPF relative to the position of Site

458   U1356. This would allow a higher connectivity between the site and the lower

459   latitudes, and promote preservation of carbonate on the sea floor. Also, such an

460   oceanographic setting would be in line with reduced sea ice along the Wilkes Land

461   margin.

462   The separate averaging of dinocyst assemblages for glacial and interglacial

463   facies from Site U1356 (Figure 7) allows us to reconstruct glacial-interglacial changes

464   in surface-water conditions throughout the Oligocene. First of all, our observations

465   suggest that Oligocene glacial-interglacial cycles were connected to substantial

466   paleoceanographic dynamics off Wilkes Land. In agreement with the 2–3 °C SST

467   variability as documented for this site during glacial-interglacial cycles (Hartman et

468   al., submitted, this volume), dinocyst assemblages contain more oligotrophic,

469   temperate dinocysts during interglacial times compared to glacial times when more

470   eutrophic, colder dinocysts proliferated (Fig. 7). This could be the result of a slight

471   latitudinal movement of oceanic frontal systems (notably the AAPF) as it has been

472   reconstructed for the Southern Ocean fronts during the most recent glacial to

473   interglacial transition (e.g., Bard and Rickaby, 2009; Kohfeld, et al., 2013; Xiao et al.,

474   2016). In such a scenario, the AAPF would reach a southern position during

475   interglacials, allowing for temperate oligotrophic surface waters to reach the site,

476 while it would migrate northward over Site U1356 during glacials, thereby causing

477 cold, high-nutrient surface-water conditions and obstructing low-latitude influence.

478

479   5.2 Implications for Oligocene–Miocene ocean circulation

480 At Site U1356, dinocyst assemblages bear similarities to present-day proximal-

481 Antarctic assemblages (Prebble et al., 2013) only in the lowermost Oligocene and in

482 strata deposited after the mid-Miocene Climate Optimum (after 14.2 Ma); in

483 particular, they are characterized by high abundances (up to 39%) of *Selenopemphix*

484 *antarctica*. Even in those intervals, however, the relative abundances of *S. antarctica*

485 do not reach present-day values at the same site (Prebble et al., 2013). The absence of

486 a strong shift towards modern-day-like assemblages in our record can be interpreted

487 to reflect a weaker-than-present ACC. This interpretation is in line with numerical

488 models (Herold et al., 2012; Hill et al., 2013). The ACC itself represents an important

489 barrier for latitudinal surface-water transport towards the Antarctic margin, in

490 addition to the Antarctic Divergence (Olbers et al., 2004). Our data suggest an

491 increase in the influence of oligotrophic dinocysts at the Antarctic margin during the

492 late Oligocene and during the MMCO, which argues against the installation of a

493 vigorous ACC at 30 Ma as recently inferred by Scher et al. (2015): No particular

494 change in sea-surface conditions emerges from our dinoflagellate cyst data around 30

495 Ma, and there is no major change in the benthic $\delta^{18}O$ data either (Figure 5). Instead, if

496 the Tasmanian Gateway had opened to an extent that allowed ACC development

497 (Scher et al., 2015), the ACC must have been much weaker throughout the Oligocene

498 and Miocene than at present, which has also emerged from modelling experiments

499 (Hill et al., 2013). The strongly different dinocyst assemblages compared to present-

500 day nearby Site U1356 throughout our record imply that a strong coherent ACC was

501 not installed until after the mid-Miocene Climatic Transition (MMCT; 11 Ma). This is

502 consistent with inferences from the lithology at the same site (Salabarnada et al.,

503 submitted, this volume), suggesting a proto-ACC much weaker than at present and,

504 likewise, weaker Southern Ocean frontal systems. An alternative explanation is that

505 the ACC increased in strength during the Oligocene–Miocene, but that this

506 strengthening had no influence on the dinocyst assemblages at Site U1356. However,

507 the vigorous nature of the ACC influencing surface as well as bottom waters and

508 governing eddy water circulation in the Southern Ocean (Olbers et al., 2004) in

509 combination with the high sensitivity of dinoflagellates to changes in surface-water

510 conditions (e.g., Zonneveld et al., 2013; Prebble et al., 2013) makes such a scenario

511 very unlikely. Nevertheless, to firmly clarify whether the ACC reached its present-day

512 strength only after the MMCT (as suggested by our data), ocean-circulation modelling

513 of time slices younger than the Oligocene (Hill et al., 2013) will be required.

514   Our results also seem difficult to reconcile with indications of bottom-water

515 formation at the Wilkes Land margin, as seen from neodymium isotope analyses on

516 the same sediments (Huck et al., 2017). It could be that bottom water formation took

517 place only when surface waters cooled down in wintertime, and the organic proxies

518 are more representative of spring/summer conditions. Salabarnada et al. (this

519 volume) interpret bottom-current activity in the Oligocene at Site U1356 and suggest

520 it may be spilling over from the Ross Sea, like today. Our dinocyst results and the SST

521 reconstructions by Hartman et al. (submitted this volume) suggest that surface

522 waters at the Wilkes Land margin were too warm to allow local bottom-water

523 formation, therefore our data also supports the suggestion that bottom water along

524 the Wilkes Land margin was sourced from the Ross Sea.

525

526   5.3 Implications for ice-sheet and sea-ice variability

527 The relative abundances of the sea-ice-related *Selenopemphix antarctica* are

528 consistently lower in our record than in present-day dinocyst assemblages nearby

529 Site U1356 (Prebble et al., 2013; Figure 3). This suggests that sea-ice conditions were

530 never similar to today during the studied time interval. More specifically, our

531 dinocysts suggest the occurrence of sea ice near the site only during two time

532 intervals: The first 1.5 million years following the Oi-1 glaciation (33.6–32.1 Ma;

533 Figure 5), and during and after the mid-Miocene climatic Transition (after 14.2 Ma;

534 Figure 5). Numerical ice-sheet/sea-ice modelling (DeConto et al., 2007) has suggested

535 sea-ice to develop only if the continental ice sheets reach the coastline. Our lack of

536 sea-ice indicators during most of the Oligocene and Miocene could thus point towards

537 a much-reduced Antarctic continental ice sheet during that time. The finding of a

538 weaker sea-ice season throughout most of the Oligocene–Miocene at Site U1356 is

539 important because it suggests a decrease in the potential formation of Antarctic

540 bottom waters at this site.

541   The relative abundance of oligotrophic dinocyst taxa broadly follows long-

542 term Oligocene-Miocene benthic $\delta^{18}O$ trends (see Fig. 5): During times of low $\delta^{18}O$

543 values in deep-sea benthic foraminifera (and thus high deep-sea temperatures and/or

544 less ice volume; e.g., at 32 Ma, 24 Ma and 15 Ma; Figure 5), the abundance of

545 oligotrophic temperate dinocysts was high (Figure 5). At times of higher $\delta^{18}O$ values,

546 lower deep-sea temperatures and higher ice volume (e.g., at 33.5 Ma, 27 Ma, 23 Ma,

547 and 13 Ma; Figure 5), temperate dinocysts were reduced in abundance and high-

548 nutrient, sea-ice indicators (re)appeared. Altogether, on long time scales this pattern

549 suggests that there was a stronger influence of warm surface waters at the Wilkes

550 Land margin at times when ice sheets were smaller and climate was warmer, and less

551 influence of warm surface waters during times of larger ice sheets. Hence a

552 connection existed between ice- sheet expansion/retreat and paleoceanography.

553   Oxygen-isotope mass-balance calculations suggest that a modern-day-sized

554 Antarctic ice sheet formed at the Eocene/Oligocene boundary (DeConto et al., 2008).

555 Benthic $\delta^{18}O$ records suggest that ice sheets must have fluctuated considerably in size

556 during the subsequent Oligocene and Miocene (Liebrand et al., 2017), although this

557 inference lacks an independent assessment of the deep-sea temperature effect in

558 these $\delta^{18}O$ values. The same conclusion was reached based on detailed microfossil,

559 geochemical and facies analyses on sediments from the Gippsland Basin, southeast

560 Australia (Gallagher, et al. 2013). This study suggests that ice volume during the early

561 Oligocene varied by as much as 140–40% of its present-day size, of which the

562 maximum ice volume estimates far exceed those implied by our data. However, there

563 is consistency in the observation of considerable glacial-interglacial and long-term

564 dynamics in the ice-ocean system. This is in contrast to the heavy $\delta^{18}O$ values for

565 Oligocene benthic foraminifera from Maud Rise (ODP Site 690), which lead to suggest

566 Antarctic ice sheets were near-present-day size throughout the Oligocene

567 (Hauptvogel et al., 2017). It remains to be seen whether the variability in

568 paleoceanography as indicated by our data can be extrapolated to larger parts of the

569 Antarctic margin, including regions of deep-water formation. Given the high

570 temperatures and only weak sea-ice influence, the Wilkes Land margin was likely not

571   the primary sector of deep-water formation (see, e.g., Herold et al., 2012), although

572   there is ample evidence for bottom-current activity at the site (Salabarnada et al.,

573   submitted, this volume; Huck et al., 2017). Instead, it appears that bottom-water

574   formation during the Oligocene was taking place along the Wilkes Land coast (Huck,

575   et al. 2017). If the oceanographic and climate variability that we reconstruct offshore

576   Wilkes Land also characterises regions of deep-water formation, some (if not all) of

577   the variability both on long and on orbital time scales as documented in benthic $\delta^{18}O$

578   records would be due to changes in deep-sea temperature rather than Antarctic ice

579   volume (see also Hartman et al., submitted, this volume). Meanwhile, we find little

580   support in our study for the large (and, by implication, marine-terminating)

581   continental ice sheets in this sector of East Antarctica during the Oligocene as implied

582   by Hauptvogel et al. (2017) given the absence of dominance of sea-ice dinocysts and

583   the presence of in situ terrestrial palynomorphs (Strother et al., 2017). As an

584   alternative explanation for the difference in $\delta^{18}O$ values between Maud Rise (Site

585   690) and the equatorial Pacific (Site 1218) during the Oligocene (Hauptvogel et al.,

586   2017), we suggest that these two sedimentary archives have recorded the

587   characteristics of two different deep-water masses, with those at Maud Rise (Site

588   690) being much colder and more saline than those in the equatorial Pacific (Site

589   1218).

590

591   **6. Conclusions**

592   The dinocyst assemblages in the Oligocene–Miocene (33.6–11 Ma) of Site U1356 were

593   interpreted in terms of surface-water paleoceanography via comparison with

594   present-day dinocyst distribution patterns. Based on our results, we suggest that the

595 Oligocene–Miocene surface paleoceanography of the Southern Ocean was

596 fundamentally different from that of today. A sea-ice signal (yet still weaker than at

597 present) emerges for the Wilkes Land margin only for the first 1.5 million years of the

598 Oligocene (33.6–32.1 Ma) and during and after the mid-Miocene climatic transition

599 (after 14.2 Ma). During the remainder of the Oligocene–Miocene, surface waters off

600 Wilkes Land were warm and relatively oligotrophic; notably, they lack indications of

601 a prominent sea-ice season. Upwelling at the Antarctic Divergence was profoundly

602 weaker during Oligocene and Miocene times than at present, or significantly

603 displaced southward from its present-day position. Furthermore, the continental ice

604 sheets were much reduced at the Wilkes Land sub-glacial basin for most of the

605 Oligocene–Miocene compared to today. The influence of warm oligotrophic surface

606 waters appears strongly coupled to deep-sea $\delta^{18}O$ values, suggesting enhanced low-

607 latitude influence of surface waters during times of light $\delta^{18}O$ in the deep sea and *vice*

608 *versa*. The absence of (a trend towards a stronger) paleoceanographic isolation of the

609 Wilkes Land margin throughout the Oligocene to mid-Miocene suggests that the ACC

610 may not have attained its full, present-day strength until at least after the mid-

611 Miocene Climatic transition. Moreover, we note considerable glacial-interglacial

612 amplitude variability in this oceanographic setting. Stronger influence of oligotrophic,

613 low-latitude-derived surface waters prevailed over Site U1356 during interglacial

614 times and more eutrophic, colder waters during glacial times. This pattern may

615 suggest considerable latitudinal migration of the AAPF over the course of Oligocene

616 and Miocene glacial-interglacial cycles.

617

618 **Acknowledgements**

619   This research used data and samples from the Integrated Ocean Drilling Program

620   (IODP). IODP was sponsored by the U.S. National Science Foundation and

621   participating countries under management of Joined Oceanographic Institutions Inc.

622   PKB and FS thank NWO-NNPP grant no 866.10.110, NWO-ALW VENI grant no

623   863.13.002 for funding and Natasja Welters for technical support. JP acknowledges

624   support through the IODP priority program of the German Research Foundation

625   (DFG). CE and AS thank the Spanish Ministerio de Economía y Competitividad for

626   Grant CTM2014-60451-C2-1-P. We thank Kasia Śliwińska, Stephen Gallagher and an

627   anonymous reviewer for their constructive comments that considerably improved

628   our manuscript.

629

630   Author contributions

631   PKB, FS, CE, and JP designed the research. AJPH, FS and PKB carried out dinocyst

632   analyses for the earliest Oligocene, Miocene, and Oligocene-Miocene boundary

633   interval, respectively. AS and CE provided the lithological data. PKB integrated, cross-

634   validated and compiled the data, and wrote the paper with input from all co-authors.

635

636

637 **Figure captions**

638 Figure 1. Paleogeography of the Southwest Pacific Ocean and position of IODP Site

639 U1356 (red star) at (a) 0 Ma, (b) 10 Ma, (c) 20 Ma, and (d) 30 Ma. Figures are

640 modified after Bijl et al. (2018). Reconstructions were adapted from G-plates, with

641 plate circuit from Seton et al. (2012) and absolute plate positions of Torsvik et al.

642 (2012).

643

644 Figure 2. Age model for the Oligocene–Miocene interval of Hole U1356A. Core

645 recovery, lithostratigraphic facies after Salabarnada et al. (this volume; see also

646 Sangiorgi et al., 2018) and lithostratigraphic units (Escutia et al., 2011), Samples

647 taken for palynology and age-depth plot (tie points were derived from Tauxe et al.,

648 2012, which has been recalibrated to the GTS2012 time scale of Gradstein et al., 2012

649 and modified based on Crampton et al., 2016)). Grey intervals in paleomagnetic data

650 reflect unknown paleomagnetic orientation, either due to absence of core recovery or

651 poor signal. (o) = old end; (y) = young end. Figure modified from Bijl et al. (2018).

652

653 Figure 3. Generic representation of present-day distributions of dinocysts in surface

654 sediments in the Southern Ocean. The dinocyst pie charts represent average dinocyst

655 assemblage compositions for surface sediments underneath oceanic frontal zones in

656 the Southern Ocean. Figure modified from Sangiorgi et al. (2018), data replotted from

657 Prebble et al. (2013).

658

659 Figure 4. Core recovery and lithostratigraphic facies (after Salabarnada et al., this

660 volume, and Sangiorgi et al., 2018) and lithologic units (Escutia et al., 2011),

661   chronostratigraphic epochs (E = Eocene) and stages (L = Lutetian, Burd. =

662   Burdigalian, Ser. = Serravallian, T. = Tortonian), absolute palynomorph (grey) and in

663   situ dinocyst (black) concentrations (# per gram of dry sediment, presented on a

664   logarithmic scale), palynomorph content (reworked dinocysts, in situ dinocysts,

665   acritarchs, terrestrial palynomorphs (given in percentages of total palynomorphs),

666   and relative abundance of in situ dinocyst eco-groups (in percentage of in situ

667   dinocysts) for the Oligocene–Miocene of Hole U1356A.

668

669   Figure 5. Compilation of benthic foraminiferal oxygen isotope data from Site 588

670   (Zachos et al., 2008), Site 1090 (Zachos et al., 2008) Site 1218 (Pälike et al., 2006), ,

671   Sites 1264/1265 (Liebrand et al., 2017), Site U1334 (Holbourn et al., 2015), Site

672   U1337 (Beddow et al., 2016), all calibrated to the GTS2012 time scale (Gradstein et

673   al., 2012) with in situ dinocyst assemblage data from Site U1356 (see Fig. 4 for

674   legend). For presentation of the dinocyst data (see Fig. 4 for legend), the age-depth

675   model specified in Figure 2 and Table 1 was used.

676

677   Figure 6. Comparison of absolute (left bar, in # * gr $^{-1}$ dry weight) and relative (right

678   bar; in % of total palynomorphs) abundances of palynomorph groups per lithology

679   for Hole U1356A. Average (black lines) and 17–83% percentile (coloured bar) of

680   absolute and relative abundances of total palynomorphs, reworked dinocysts, in situ

681   dinocysts, acritarchs, and terrestrial palynomorphs grouped for the different facies

682   (Salabarnada et al., submitted this volume).

683

684   Figure 7. Abundance/concentration of in situ eco-groups within various lithologies at

685   Hole U1356A. Average (black line) and 17–83% percentile (coloured bar) of relative

686   abundances of grouped taxa from samples from the different facies (Salabarnada et

687   al., submitted this volume).

688

689   **Table captions**

690   Table 1. Age constraints for the Oligocene–Miocene of Hole U1356A.

691   Table 2. List of assumed in situ and reworked dinoflagellate cyst taxa encountered in

692   this study. See Bijl et al. (2018) for informal species descriptions and discussion about

693   which species are considered reworked and in situ.

694

695   References

696   Badger, M. P. S., Lear, C. H., Pancost, R. D., Foster, G. L., Bailey, T. R., Leng, M. J., Abels, H.
697   A.: CO$_2$ drawdown following the middle Miocene expansion of the Antarctic Ice Sheet,
698   Paleoceanography, 28, 42-53, 2013.

699   Bard, E. and Rickaby, R. E. M.: Migration of the subtropical front as a modulator of glacial
700   climate. Nature. 460, 380-383, 2009.

701   Barker, P., Camerlenghi, A., Acton, G., Brachfeld, S., Cowan, E., Daniels, J., Domack, E., Escutia,
702   C., Evans, A., Eyles, N., Guyodo, Y., Iorio, M., Iwai, M., Kyte, F., Lauer, C., Maldonado, A.,
703   Moerz, T., Osterman, L., Pudsey, C., Schuffert, J., Sjunneskog, C., Vigar, K., Weinheimer, A.,
704   Williams, T., Winter, D., Wolf-Welling, T.: Antarctic glacial history and sea-level change - Leg
705   178 samples Antarctic Peninsula margin sediments, JOIDES Journal 24, 7-10, 1998.

706   Barker, P. F., Barrett, P. J., Cooper, A. K., Huybrechts, P.: Antarctic glacial history from numerical
707   models and continental margin sediments, Palaeogeography, Palaeoclimatology, Palaeoecology,
708   150, 247-267, 1999.

709   Barker, P. F. and Thomas, E.; Origin, signature and paleoclimatic influence of the Antarctic
710   Circumpolar Current, Earth Science Reviews, 66, 143-162, 2004

711   Barrett, P. J.: Antarctic Cenozoic history from the CIROS-1 drillhole, McMurdo Sound. Science
712   Information Publishing Centre DSIR Bulletin, volume 245, Wellington, 1989.

713   Beddow, H. M., Liebrand, D., Sluijs, A., Wade, B. S., Lourens, L. J.: Global change across the
714   Oligocene-Miocene transition: High-resolution stable isotope records from IODP Site U1334
715   (equatorial Pacific Ocean), Paleoceanography, 31, 81-97, 2016.

716   Bijl, P. K., Bendle, A. P. J., Bohaty, S. M., Pross, J., Schouten, S., Tauxe, L., Stickley, C. E.,
717   McKay, R. M., Röhl, U., Olney, M., Sluijs, A., Escutia, C., Brinkhuis, H., Expedition 318
718   scientists; Eocene cooling linked to early flow across the Tasmanian Gateway, Proceedings of the
719   National Academy of Sciences of the United States of America, 110, 9645-9650, 2013a.

720   Bijl, P.K., Houben, A.J.P., Bruls, A., Pross, J., Sangiorgi, F.: Stratigraphic calibration of
721   Oligocene–Miocene organic-walled dinoflagellate cysts from offshore Wilkes Land, East
722   Antarctica, and a zonation proposal: Journal of Micropaleontology, 37(1), pp. 105-138, 2018.

723   Bijl, P.K., Houben, A.J.P., Schouten, S., Bohaty, S.M., Sluijs, A., Reichart, G.J., Sinninghe
724   Damsté, J.S., Brinkhuis, H.: Transient Middle Eocene Atmospheric Carbon Dioxide and
725   Temperature Variations, Science, 330, 819-821, 2010.

726   Bijl, P. K., Pross, J., Warnaar, J., Stickley, C. E., Huber, M., Guerstein, R., Houben, A. J. P., Sluijs,
727   A., Visscher, H., Brinkhuis, H.: Environmental forcings of Paleogene Southern Ocean
728   dinoflagellate biogeography. Paleoceanography, 26, PA1202, 2011.

729   Bijl, P. K., Sluijs, A., Brinkhuis, H.: A magneto- chemo- stratigraphically calibrated dinoflagellate
730   cyst zonation of the early Paleogene South Pacific Ocean. Earth-Science Reviews, 124, 1-31,
731   2013b.

732   Boessenkool, K. P., Van Gelder, M., Brinkhuis, H., Troelstra, S. R.: Distribution of organic-walled
733   dinoflagellate cysts in surface sediments from transects across the Polar Front offshore southeast
734   Greenland, J. Quaternary Sci., 16, 661–666, 2001.

735   Brinkhuis, H., Munsterman, D. M., Sengers, S., Sluijs, A., Warnaar, J., Williams, G. L.: Late
736   Eocene to Quaternary dinoflagellate cysts from ODP Site 1168, off western Tasmania, in: Exon,

737 N., Kennett, J. P. (Eds.), Proceedings of the Ocean Drilling Program, Scientific Results, volume
738 189, U.S. Government Printing Office, College Station, Texas, 2003a.

739 Brinkhuis, H., Sengers, S., Sluijs, A., Warnaar, J., Williams, G. L.: Latest Cretaceous to earliest
740 Oligocene, and Quaternary dinoflagellates from ODP Site 1172, East Tasman Plateau, in: Exon, N.,
741 Kennett, J. P. (Eds.), Proceedings of the Ocean Drilling Program, Scientific Results, volume 189.
742 U.S. Government Printing Office, College Station, Texas, 2003b.

743 Close, D. I., Watts, A. B., Stagg, H. M. J.: A marine geophysical study of the Wilkes Land rifted
744 continental margin, Antarctica, Geophysical Journal International, 177, 430-450, 2009.

745 Cook, C. P., Van De Flierdt, T., Williams, T., Hemming, S. R., Iwai, M., Kobayashi, M., Jimenez-
746 Espejo, F. J., Escutia, C., González, J. J., Khim, B., McKay, R. M., Passchier, S., Bohaty, S. M.,
747 Riesselman, C. R., Tauxe, L., Sugisaki, S., Galindo, A. L., Patterson, M. O., Sangiorgi, F., Pierce,
748 E. L., Brinkhuis, H., Klaus, A., Fehr, A., Bendle, J. A. P., Bijl, P. K., Carr, S. A., Dunbar, R. B.,
749 Flores, J. A., Hayden, T. G., Katsuki, K., Kong, G. S., Nakai, M., Olney, M. P., Pekar, S. F., Pross,
750 J., Röhl, U., Sakai, T., Shrivastava, P. K., Stickley, C. E., Tuo, S., Welsh, K., Yamane, M.:
751 Dynamic behaviour of the East Antarctic ice sheet during Pliocene warmth, Nature Geoscience, 6,
752 765-769, 2013.

753 Cooper, A. K. and O'Brien, P. E.: Leg 188 synthesis: Transitions in the glacial history of the Prydz
754 Bay region, East Antarctica, from ODP drilling, Proceedings of the Ocean Drilling Program:
755 Scientific Results, 188, 1-42, 2004.

756 Crampton, J. S., Cody, R. D., Levy, R., Harwood, D., McKay, R., Naish, T. R.: Southern Ocean
757 phytoplankton turnover in response to stepwise Antarctic cooling over the past 15 million years.
758 Proceedings of the National Academy of Sciences of the United States of America, 113, 6868-
759 6873, 2016.

760 DeConto, R. M., Pollard, D., Harwood, D.: Sea-ice feedback and Cenozoic evolution of Antarctic
761 climate and ice sheets, Paleoceanography, 22, PA3214, 2007.

762 DeConto, R. M., Pollard, D., Wilson, P. A., Pälike, H., Lear, C. H., Pagani, M.: Thresholds for
763 Cenozoic bipolar glaciation, Nature, 455, 652-657, 2008.

764 Egger, L. M., Bahr, A., Friedrich, O., Wilson, P. A., Norris, R. D., van Peer, T. E., Lippert, P. C.,
765 Liebrand, D., Pross, J.: Sea-level and surface-water change in the western North Atlantic across the
766 Oligocene–Miocene Transition: a palynological perspective from IODP Site U1406 (New-
767 foundland margin), Marine Micropaleontology, 139, 57-71, 2018.

768 Escutia, C., Brinkhuis, H.: From Greenhouse to Icehouse at the Wilkes Land Antarctic Margin:
769 IODP Expedition 318 Synthesis of Results, Developments in Marine Geology, 7, pp. 295-328,
770 2014.

771 Escutia, C., Brinkhuis, H., Klaus, A. and Expedition 318 Scientists; Proceedings of the Integrated
772 Ocean Drilling Program, Initial Results, volume 318, Tokyo (Integrated Ocean Drilling Program
773 Management International, Inc.), 2011.

774 Esper, O. and Zonneveld, K. A. F.: The potential of organic-walled dinoflagellate cysts for the
775 reconstruction of past sea-surface conditions in the Southern Ocean, Marine Micropaleontology,
776 65, 185-212, 2007.

777 Esper, O. and Zonneveld, K. A. F.: Distribution of organic-walled dinoflagellate cysts in surface
778 sediments of the Southern Ocean (eastern Atlantic sector) between the Subtropical Front and the
779 Weddell Gyre, Marine Micropaleotology, 46, 177-208, 2002.

780 Exon, N. F., Kennet, J. P., Malone, M.: Leg 189 Synthesis: Cretaceous- Holocene history of the
781 Tasmanian Gateway. In Exon, N.F., Kennett, J.P., and Malone, M.J. (Eds.), Proceedings of the
782 Ocean Drilling Program, Scientific Results, Volume 189, 2004.

783 Eynaud, F., Giraudeau, J., Pichon, J., Pudsey, C. J.: Sea-surface distribution of coccolithophores,
784 diatoms, silicoflagellates and dinoflagellates in the South Atlantic Ocean during the late austral
785 summer 1995, Deep-Sea Research Part I: Oceanographic Research Papers, 46, 451-482, 1999.

786 Foster, G. L., Lear, C. H., Rae, J. W. B.: The evolution of pCO_2, ice volume and climate during the
787 middle Miocene, Earth and Planetary Science Letters, 341-344, 243-254, 2012.

788 Foster, G. L. and Rohling, E. J.: Relationship between sea level and climate forcing by CO_2 on
789 geological timescales, Proceedings of the National Academy of Sciences of the United States of
790 America, 110, 1209-1214, 2013.

791 Fretwell, P., Pritchard, H. D., Vaughan, D. G., Bamber, J. L., Barrand, N. E., Bell, R., Bianchi, C.,
792 Bingham, R. G., Blankenship, D. D., Casassa, G., Catania, G., Callens, D., Conway, H., Cook, A.
793 J., Corr, H. F. J., Damaske, D., Damm, V., Ferraccioli, F., Forsberg, R., Fujita, S., Gim, Y.,
794 Gogineni, P., Griggs, J. A., Hindmarsh, R. C. A., Holmlund, P., Holt, J.W., Jacobel, R. W.,
795 Jenkins, A., Jokat, W., Jordan, T., King, E. C., Kohler, J., Krabill, W., Riger-Kusk, M., Langley, K.
796 A., Leitchenkov, G., Leuschen, C., Luyendyk, B. P., Matsuoka, K., Mouginot, J., Nitsche, F. O.,
797 Nogi, Y., Nost, O. A., Popov, S.V., Rignot, E., Rippin, D. M., Rivera, A., Roberts, J., Ross, N.,
798 Siegert, M. J., Smith, A.M., Steinhage, D., Studinger, M., Sun, B., Tinto, B.K., Welch, B.C.,
799 Wilson, D., Young, D. A., Xiangbin, C., Zirizzotti, A.: Bedmap2: Improved ice bed, surface and
800 thickness datasets for Antarctica, Cryosphere, 7, 375-393, 2013.

801 Gallagher, S. J., Villa, G., Drysdale, R. N., Wade, B. S., Scher, H., Li, Q., Wallace, M. W.,
802 Holdgate, G. R.: A near-field sea level record of east Antarctic ice sheet instability from 32 to 27
803 Myr. Paleoceanography. 28, 1-13, 2013.

804 Gradstein, F. M., Ogg, J. G., Schmitz, M. D., Ogg, G. M.: The Geologic Time Scale 2012, 1-2, 1-
805 1144, Elsevier, Amsterdam, the Netherlands, 2012.

806 Gradstein, F. M., Ogg, J. G., Smith, A. G.: A geologic timescale 2004, Cambridge University
807 Press, Cambridge, 2004.

808 Greenop, R., Foster, G. L., Wilson, P. A., Lear, C. H.: Middle Miocene climate instability
809 associated with high-amplitude CO_2 variability, Paleoceanography, 29, 845-853, 2014.

810 Hartman, J. D., Sangiorgi, F., Salabarnada, A., Peterse, F., Houben, A. J. P., Schouten, S., Escutia,
811 C., and Bijl, P. K.: Oligocene TEX_{86}-derived seawater temperatures from offshore Wilkes Land
812 (East Antarctica), Clim. Past Discuss., https://doi.org/10.5194/cp-2017-153, in review, 2017.

813 Harland, R. and Pudsey, C. J.:Dinoflagellate cysts from sediment traps deployed in the Bellingshausen,
814 Weddell and Scotia seas, Antarctica. Marine Micropaleontology. 37, 77-99, 1999..

815 Harwood, D., Levy, R., Cowie, J., Florindo, F., Naish, T., Powell, R., Pyne, A.: Deep drilling with
816 the ANDRILL program in Antarctica, Scientific Drilling, 1, 43-45, 2006.

817 Hauptvogel, D. W., Pekar, S. F., Pincay, V.: Evidence for a heavily glaciated Antarctica during the
818 late Oligocene "warming" (27.8-24.5): stable isotope records from ODP Site 690,
819 Paleoceanography, PA002972, 384-384-396, 2017.

820 Herold, N., Huber, M., Müller, R. D.: Modeling the Miocene Climatic Optimum. Part I: Land and
821 atmosphere, Journal of Climate 24, 6353-6373, 2011.

822 Herold, N., Huber, M., Müller, R. D., Seton, M.: Modeling the Miocene Climatic Optimum: Ocean
823 circulation, Paleoceanography 27, PA1209, 2012.

824 Hill, D. J., Haywood, A. M., Valdes, P. J., Francis, J. E., Lunt, D. J., Wade, B. S., Bowman, V. C.:
825 Paleogeographic controls on the onset of the Antarctic circumpolar current, Geophysical Research
826 Letters, 40, 5199-5204, 2013.

827 Holbourn, A., Kuhnt, W., Kochhann, K. G. D., Andersen, N., Meier, K. J.: Global perturbation of
828 the carbon cycle at the onset of the Miocene Climatic Optimum, Geology, 43, 123-126, 2015.

829 Houben, A. J. P.: Triggers and Consequences of glacial expansion across the Eocene-Oligocene
830 transition. LPP contributions series no. 39, PhD thesis Utrecht University, Utrecht, the Netherlands,
831 2012.

832 Houben, A. J. P., Bijl, P. K., Pross, J., Bohaty, S. M., Passchier, S., Stickley, C. E., Röhl, U.,
833 Sugisaki, S., Tauxe, L., Van De Flierdt, T., Olney, M., Sangiorgi, F., Sluijs, A., Escutia, C.,
834 Brinkhuis, H.: Reorganization of Southern Ocean plankton ecosystem at the onset of Antarctic
835 glaciation, Science, 340, 341-344, 2013.

836 IPCC: Climate Change 2013: The Physical Science Basis. Contribution of Working Group I to the
837 Fifth Assessment Report of the Intergovernmental Panel on Climate Change, Cambridge
838 University Press, Cambridge, United Kingdom and New York, NY, USA, 2013.

839 Knorr, G. and Lohmann, G.: Climate warming during Antarctic ice sheet expansion at the middle
840 Miocene transition. Nature Geoscience, 7, 376-381, 2014.

841 Kohfeld, K. E., Graham, R. M., de Boer, A. M., Sime, L. C., Wolff, E. W., Le Quéré, C., Bopp, L.
842 Southern Hemisphere westerly wind changes during the Last Glacial Maximum: paleo-data
843 synthesis, Quaternary Science Reviews, 68, 76-95, 2013.

844 Lear, C. H., Rosenthal, Y. Coxall, H. K., Wilson, P. A. Late Eocene to early Miocene ice sheet
845 dynamics and the global carbon cycle, *Paleoceanography*, 19, PA4015, doi:
846 10.1029/2004PA001039, 2004.

847 Levy, R. H., Harwood, D. M.: Tertiary marine palynomorphs from the McMurdo Sound erratics,
848 Antarctica, in: Stilwell, J. D., Feldmann, R. M. (Eds.), Paleobiology and Paleoenvironments of
849 Eocene rocks, McMurdo Sound, East Antarctica, AGU Antarctic Research Series, pp. 183-242,
850 2000.

851 Liebrand, D., de Bakker, A. T. M., Beddow, H. M., Wilson, P. A., Bohaty, S. M., Ruessink, G.,
852 Pälike, H., Batenburg, S. J., Hilgen, F. J., Hodell, D. A., Huck, C. E., Kroon, D., Raffi, I., Saes, M.
853 J. M., van Dijk, A. E., Lourens, L. J.: Evolution of the early Antarctic ice ages, PNAS, 110(15),
854 3867-3872, 2017.

855 Liebrand, D., Lourens, L. J., Hodell, D. A., De Boer, B., Van De Wal, R. S. W., Pälike, H.:
856 Antarctic ice sheet and oceanographic response to eccentricity forcing during the early Miocene,
857 Climate of the Past, 7, 869-880, 2011.

858 Marret, F. and De Vernal, A., 1997. Dinoflagellate cyst distribution in surface
859 sediments of the southern Indian Ocean. Marine Micropaleontology. 29, 367-392.

860 Olbers, D., Borowski, D., Völker, C., Wölff, J.: The dynamical balance, transport and circulation of
861 the Antarctic Circumpolar Current. Antarctic Science, 16, 439-470, 2004.

862 Pälike, H., Norris, R. D., Herrle, J. O., Wilson, P. A., Coxall, H. K., Lear, C. H., Shackleton, N. J.,
863 Tripati, A. K., Wade, B. S.: The Heartbeat of the Oligocene Climate System, Science, 314, 1894-
864 1898, 2006.

865 Prebble, J. G., Crouch, E. M., Carter, L., Cortese, G., Bostock, H., Neil, H.: An expanded modern
866 dinoflagellate cyst dataset for the Southwest Pacific and Southern Hemisphere with environmental
867 associations, Marine Micropaleontology, 101, 33-48, 2013.

868 Rignot, E., Jacobs, S., Mouginot, J., Scheuchl, B.: Ice-shelf melting around Antarctica. Science,
869 341, 266-270, 2013.

870 Robert, C., Anderson, J., Armienti, P., Atkins, C., Barrett, P., Bohaty, S., Bryce, S., Claps, M.,
871 Curran, M., Davey, F. J., De Santis, L., Ehrmann, W., Florindo, F., Fielding, C., Hambrey, M.,
872 Hannah, M., Harwood, D. M., Henrys, S., Hoelscher, F., Howe, J. A., Jarrard, R., Kettler, R.,
873 Kooyman, S., Kopsch, C., Krissek, L., Lavelle, M., Levac, E., Niessen, F., Passchier, S., Paulsen,
874 T., Powell, R., Pyne, A., Rafat, G., Raine, I. J., Roberts, A. P., Sagnotti, L., Sandroni, S., Scholz,
875 E., Simes, J., Smellie, J., Strong, P., Tabecki, M., Talarico, F.M., Taviani, M., Verosub, K. L.,
876 Villa, G., Webb, P. N., Wilson, G. S., Wilson, T., Wise, S. W., Wonik, T., Woolfe, K., Wrenn, J.
877 H.: Summary of Results from CRP-1, Cape Roberts Project, Antarctica, Terra Antartica, 5, 125-
878 137, 1998.

879 Rovere, A., Raymo, M. E., Mitrovica, J. X., Hearty, P. J., O'Leary, M. J., Inglis, J. D.: The Mid-
880 Pliocene sea-level conundrum: Glacial isostasy, eustasy and dynamic topography, Earth and
881 Planetary Science Letters, 387, 27-33, 2014.

882 Salabarnada, A., Escutia, C., Röhl, U., Nelson, C. H., McKay, R., Jiménez-Espejo, F. F., Bijl, P.
883 K., Hartman, J. D., Ikehara, M., Strother, S. L., Salzmann, U., Evangelinos, D., López-Quirós, A.,
884 Flores, J. A., Sangiorgi, F., and Brinkhuis, H.: Late Oligocene obliquity-paced contourite
885 sedimentation in the Wilkes Land margin of East Antarctica: implications for paleoceanographic
886 and ice sheet configurations, Clim. Past Discuss., https://doi.org/10.5194/cp-2017-152, in review,
887 2017..

888 Sangiorgi, F., Bijl, P.K., Passchier, S., Salzmann, U., Schouten, S., McKay, R., Cody, R. D., Pross,
889 J., Van De Flierdt, T., Bohaty, S. M., Levy, R., Williams, T., Escutia, C., Brinkhuis, H.: Southern
890 Ocean warming and Wilkes Land ice sheet retreat during the mid-Miocene, Nature
891 Communications, 9 (1), art. no. 317, 2018.

892 Scher, H. D. and Martin, E. M.: Circulation in the Southern Ocean during the Paleogene inferred
893 from neodymium isotopes. Earth and Planetary Science Letters, 228, 391-405, 2004.

894 Scher, H. D., Whittaker, J. M., Williams, S. E., Latimer, J. C., Kordesch, W. E. C., Delaney, M. L.:
895 Onset of Antarctic Circumpolar Current 30 million years ago as Tasmanian Gateway aligned with
896 westerlies, Nature, 523, 580-583, 2015.

897 Seton, M., Müller, R.D., Zahirovic, S., Gaina, C., Torsvik, T., Shephard, G., Talsma, A., Gurnis,
898 M., Turner, M., Maus, S., Chandler, M.: Global continental and ocean basin reconstructions since
899 200Ma, Earth-Science Reviews, 113, 212-270, 2012.

900 Shepherd, A., Ivins, E. R., Geruo, A., Barletta, V. R., Bentley, M. J., Bettadpur, S., Briggs, K. H.,
901 Bromwich, D. H., Forsberg, R., Galin, N., Horwath, M., Jacobs, S., Joughin, I., King, M. A.,
902 Lenaerts, J. T. M., Li, J., Ligtenberg, S. R. M., Luckman, A., Luthcke, S.B., McMillan, M.,
903 Meister, R., Milne, G., Mouginot, J., Muir, A., Nicolas, J. P., Paden, J., Payne, A. J., Pritchard, H.,
904 Rignot, E., Rott, H., Sørensen, L. S., Scambos, T. A., Scheuchl, B., Schrama, E. J. O., Smith, B.,
905 Sundal, A. V., Van Angelen, J. H., Van De Berg, W. J., Van Den Broeke, M. R., Vaughan, D. G.,
906 Velicogna, I., Wahr, J., Whitehouse, P. L., Wingham, D. J., Yi, D., Young, D., Zwally, H. J.: A
907 reconciled estimate of ice-sheet mass balance, Science, 338, 1183-1189, 2012.

908 Sluijs, A., Brinkhuis, H., Stickley, C. E., Warnaar, J., Williams, G. L., Fuller, M.: Dinoflagellate
909 cysts from the Eocene - Oligocene transition in the Southern Ocean: Results from ODP Leg 189,
910 in: Exon, N., Kennett, J. P. (Eds.), Proceedings of the Ocean Drilling Program, Scientific Results,
911 volume 189, U.S. Government Printing Office, College Station, Texas, USA, 2003.

912 Sluijs, A., Pross, J., Brinkhuis, H.: From greenhouse to icehouse; organic walled dinoflagellate
913 cysts as paleoenvironmental indicators in the Paleogene, Earth-Science Reviews, 68, 281-315,
914 2005.

915 Stocchi, P., Escutia, C., Houben, A.J.P., Vermeersen, B.L.A., Bijl, P.K., Brinkhuis, H., DeConto,
916 R.M., Galeotti, S., Passchier, S., Pollard, D., Klaus, A., Fehr, A., Williams, T., Bendle, J.A.P.,
917 Bohaty, S.M., Carr, S.A., Dunbar, R.B., Flores, J.A., Gonzàlez, J.J., Hayden, T.G., Iwai, M.,
918 Jimenez-Espejo, F.J., Katsuki, K., Kong, G.S., McKay, R.M., Nakai, M., Olney, M.P., Pekar, S.F.,
919 Pross, J., Riesselman, C., Röhl, U., Sakai, T., Shrivastava, P.K., Stickley, C.E., Sugisaki, S., Tauxe,
920 L., Tuo, S., Van De Flierdt, T., Welsh, K., Yamane, M. Relative sea-level rise around East
921 Antarctica during Oligocene glaciation. Nature Geoscience, 6 (5), pp. 380-384, doi:
922 10.1038/ngeo1783, 2013.

923 Storkey, C. A.: Distribution of marine palynomorphs in surface sediments, Prydz Bay, Antarctica.
924 MSc thesis Victoria University of Wellington, New Zealand. http://hdl.handle.net/10063/21, 2006.

925 Strother, S. L., Salzmann, U., Sangiorgi, F., Bijl, P. K., Pross, J., Escutia, C., Salabarnada, A.,
926 Pound, M. J., Voss, J., Woodward, J.: A new quantitative approach to identify reworking in Eocene
927 to Miocene pollen records from offshore Antarctica using red fluorescence and digital imaging,
928 Biogeosciences, 14, 2089-2100, 2017.

929 Tauxe, L., Stickley, C. E., Sugisaki, S., Bijl, P. K., Bohaty, S., Brinkhuis, H., Escutia, C., Flores, J.
930 A., Iwai, M., Jimenez-Espejo, F., McKay, R., Passchier, S., Pross, J., Riesselman, C., Röhl, U.,
931 Sangiorgi, F., Welsh, K., Klaus, A., Bendle, J. A. P., Dunbar, R., Gonzalez, J., Olney, M. P., Pekar,
932 S. F., van de Flierdt, T.: Chronostratigraphic framework for the IODP Expedition 318 cores from
933 the Wilkes Land Margin: constraints for paleoceanographic reconstruction, Paleoceanography, 27,
934 PA2214, 2012.

935 Torsvik, T. H., Van der Voo, R., Preeden, U., Niocaill, C. M., Steinberger, B., Doubrovine, P. V.,
936 van Hinsbergen, D. J. J., Domeier, M., Gaina, C., Tohver, E., Meert, J. G., McCausland, P. J.,
937 Cocks, L. R. M.: Phanerozoic polar wander, palaeogeography and dynamics. Earth-Science
938 Reviews, 114, 325-368, 2012.

939 Van Hinsbergen, D. J. J., De Groot, L. V., Van Schaik, S. J., Spakman, W., Bijl, P. K., Sluijs, A.,
940 Langereis, C. G., Brinkhuis, H.: A paleolatitude calculator for paleoclimate studies. PLoS ONE,
941 10(6), e0126946, 2015.

942 Wilson, G. S., Bohaty, S. M., Fielding, C. R., Florindo, F., Hannah, M.J., Hardwood, D. M.,
943 Mcintosh, W.C., Naish, T. R., Roberts, A. P., Sagnotti, L., Scherer, R. P. , Strong, C. P., Verosub,
944 K. L., Villa, G., Webb, P. -., Woolfe, K. J.: Chronostratigraphy of CRP-2/2A, Victoria Land Basin,
945 Antarctica, Terra Antarctica 7, 647-654, 2000.

946 Wise, S. W. and Schlich, R.,. Proceedings of the Ocean Drilling Program, Scientific Results,
947 volume 120, U.S. Government Printing Office, College Station, Texas, 1992.

948 Wouters, B., Martin-Español, A., Helm, V., Flament, T., van Wessem, J. M., Ligtenberg, S. R. M.,
949 van den Broeke, M. R., Bamber, J. L.: Dynamic thinning of glaciers on the Southern Antarctic
950 Peninsula, Science 348 (6237), 899-903, 2015.

951 Wrenn, J.H. and Hart, G.F.: Paleogene dinoflagellate cyst biostratigraphy of Seymour Island,
952 Antarctica, Geological Society of America Memoires, 169, 321-447, 1988.

953 Xiao, W., Esper, O., Gersonde, R.: Last Glacial - Holocene climate variability in the Atlantic sector
954 of the Southern Ocean. Quaternary Science Reviews. 135, 115-137, 2016.

955 Zachos, J. C., Dickens, G. R., Zeebe, R. E.: An early Cenozoic perspective on greenhouse warming
956 and carbon-cycle dynamics, Nature 451, 279-283, 2008.

957 Zevenboom, D.: Dinoflagellate cysts from the Mediterranean late Oligocene and Miocene, PhD
958 thesis Utrecht University, Utrecht, the Netherlands, 1995.

959 Zonneveld, K. A. F., Marret, F., Versteegh, G. J. M., Bogus, K., Bonnet, S., Bouimetarhan, I.,
960 Crouch, E., de Vernal, A., Elshanawany, R., Edwards, L., Esper, O., Forke, S., Grøsfjeld, K.,
961 Henry, M., Holzwarth, U., Kielt, J., Kim, S., Ladouceur, S., Ledu, D., Chen, L., Limoges, A.,
962 Londeix, L., Lu, S., Mahmoud, M. S., Marino, G., Matsouka, K., Matthiessen, J., Mildenhall, D.
963 C., Mudie, P., Neil, H.L., Pospelova, V., Qi, Y., Radi, T., Richerol, T., Rochon, A., Sangiorgi, F.,
964 Solignac, S., Turon, J., Verleye, T., Wang, Y., Wang, Z., Young, M.: Atlas of modern
965 dinoflagellate cyst distribution based on 2405 data points, Review of Palaeobotany and Palynology,
966 191, 1-197, 2013.

967

a; 0 Ma

Fig. 1

b; 10 Ma

c; 20 Ma

d; 30 Ma

968

969

972

973

Fig. 4

Fig. 5
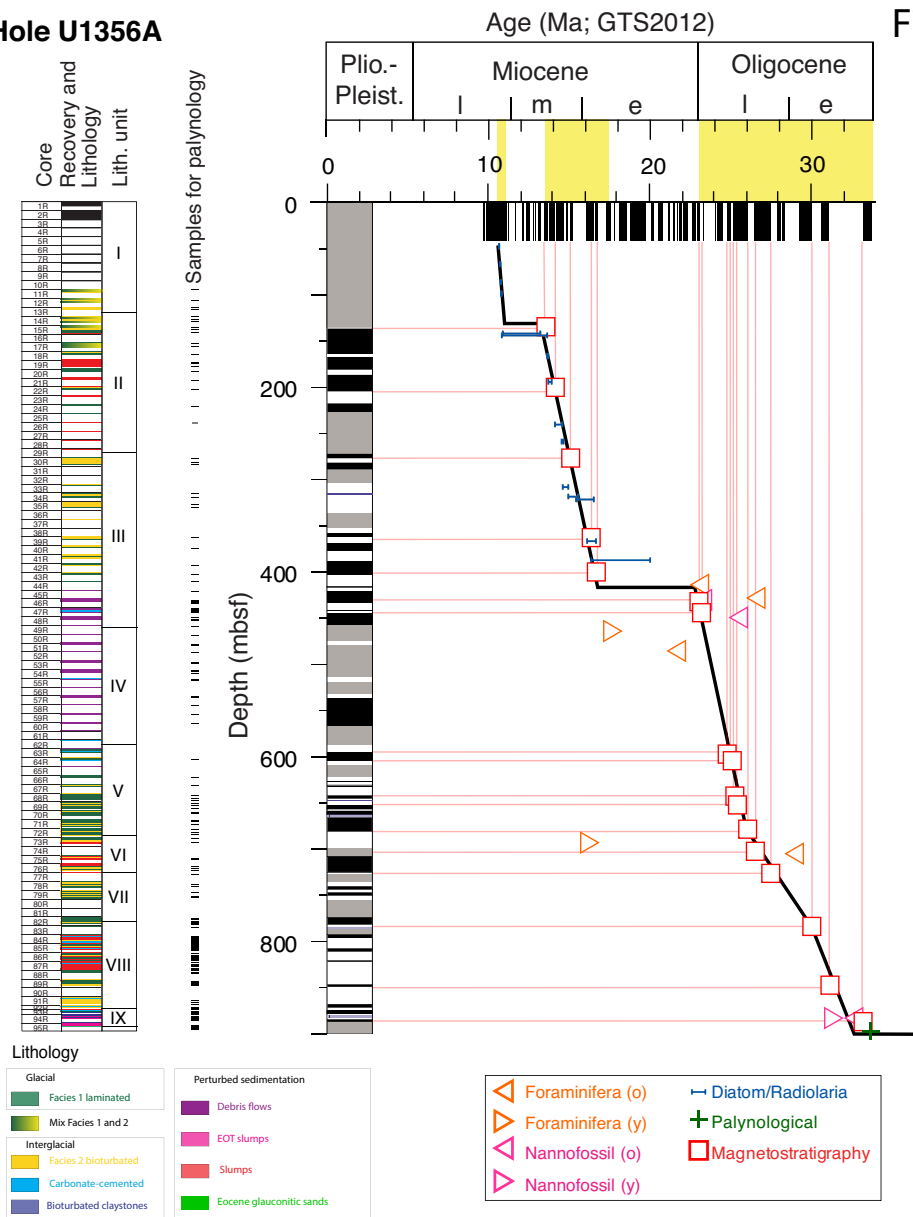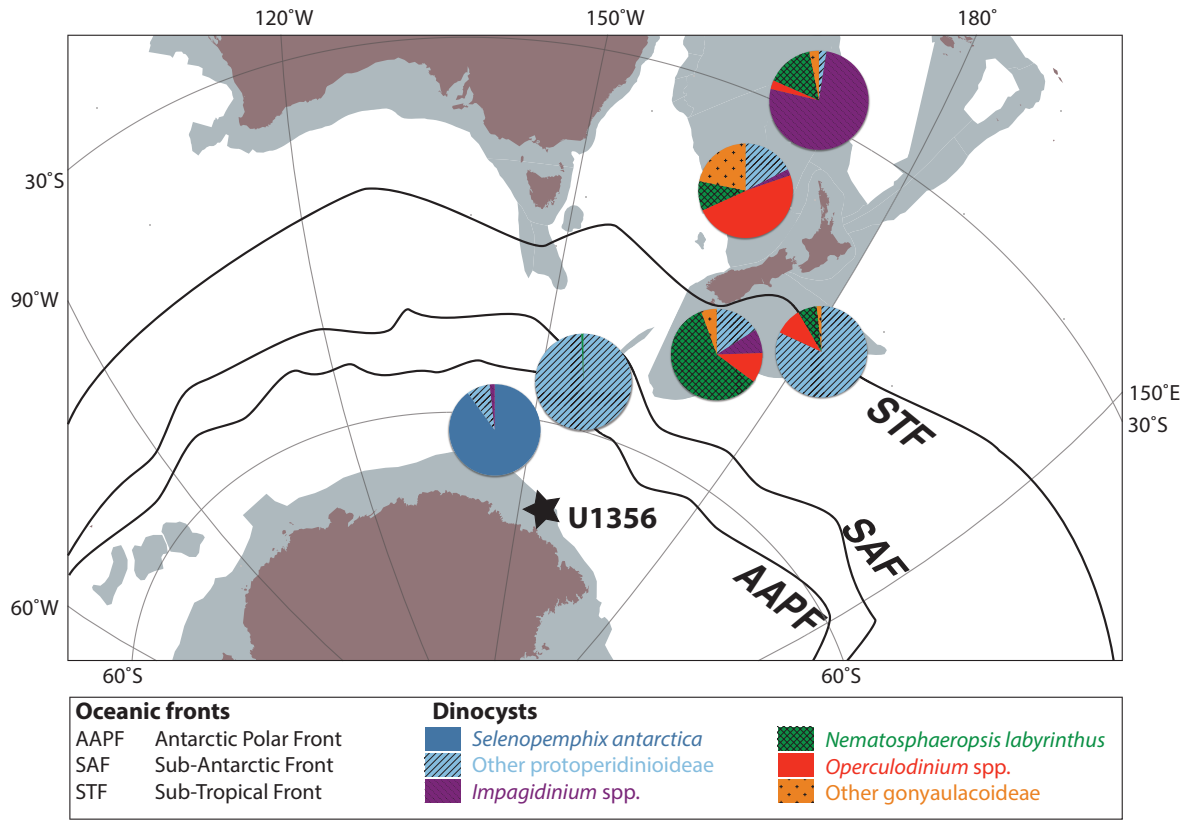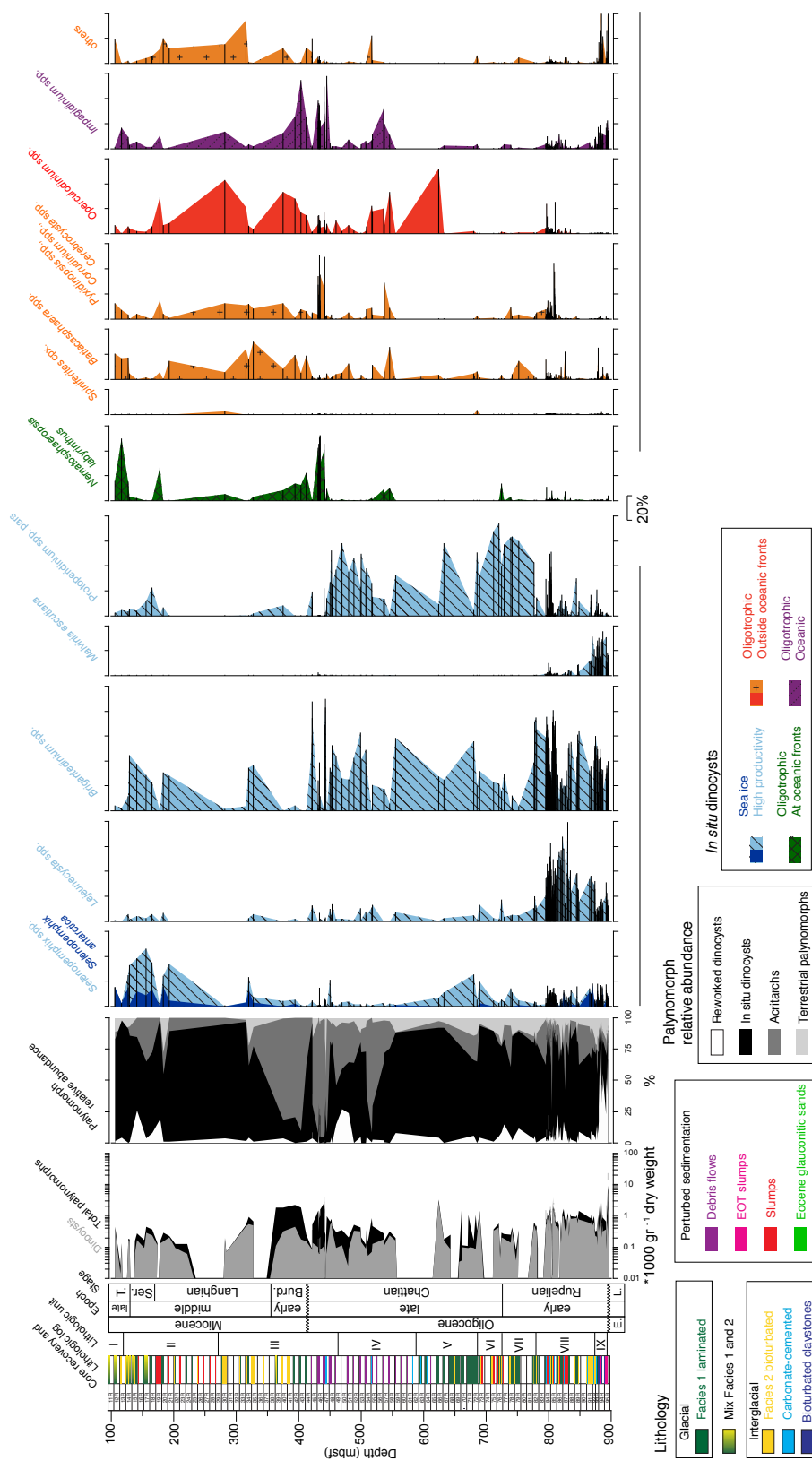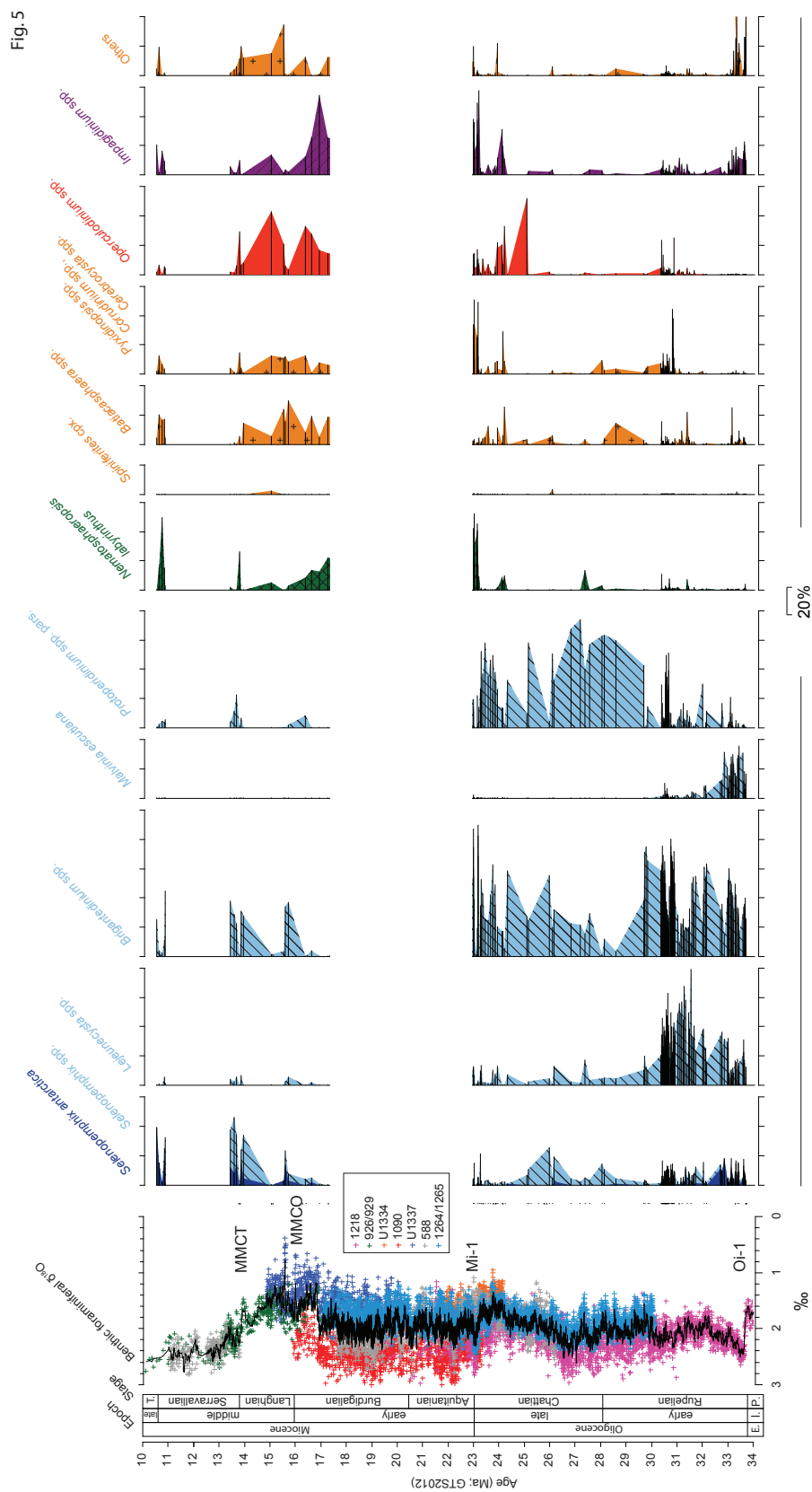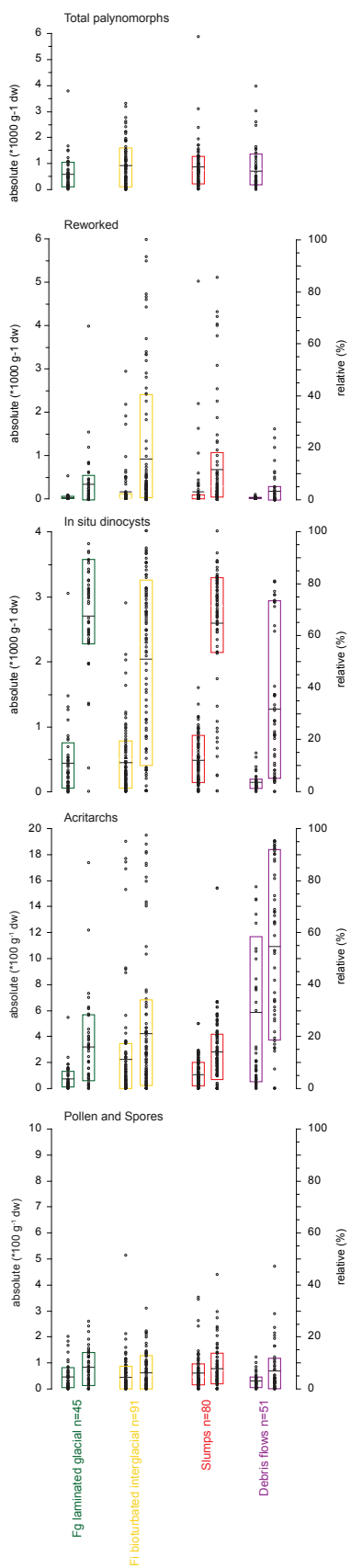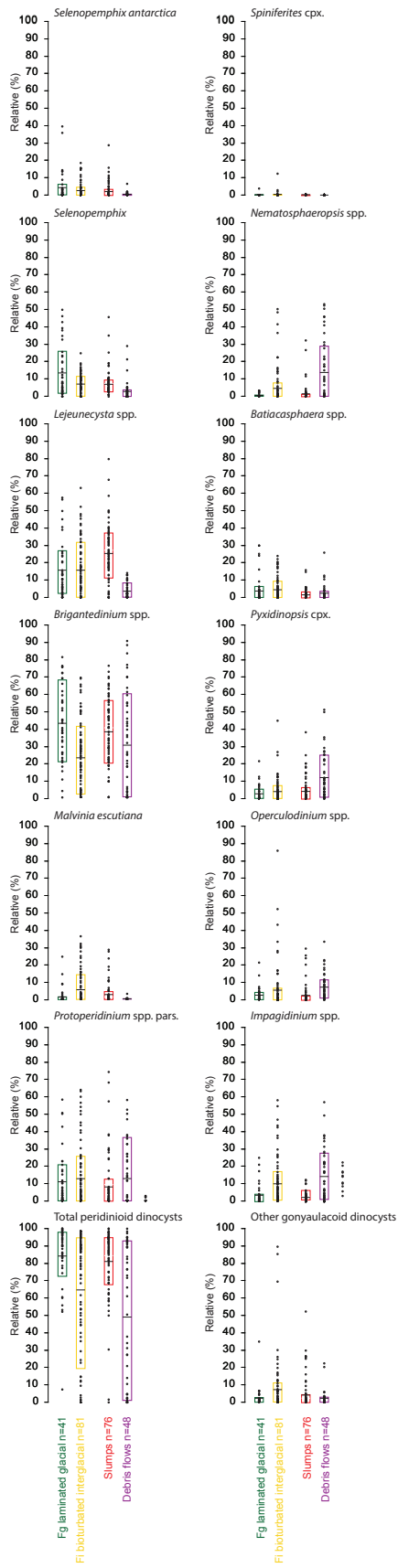
type	FO/LO	Genus, chron	(Gradstein 2(	top core	top interval	bottom core	bottom inter	depth averag	error
CONOP			10.76					98.66	
CONOP			10.92					133.80	
CONOP			13.41					133.81	
PM	(o)	C5ACn	14.07	22R-2,	75	22R-2,	90	203.23	0.07
PM	(y)	C5Bn.2n	15.03	30R-2,	50	30R-2,	75	279.63	0.13
PM	(o)	C5Cn.1n	16.27	39R-1,	35	39R-1,	65	364.10	0.15
PM	(o)	C5Cn.3n	16.72	42R-2,	59	43R-1,	25	398.28	3.98
			17.50	44R-CC		45R-CC		416.90	
			23.00	44R-CC		45R-CC		416.91	
PM	(o)	C6Cn.2n	23.03	45R-CC	40	46R-1	65	426.78	5.00
PM	(o)	C6Cn.3n	23.30	50R-1,	0			469.00	9.00
PM	(y)	C7An	24.76	63R-3,	85	63R-3,	120	597.12	0.17
PM	(o)	C7An	24.98	64R-1,	130	64R-1,	135	604.33	0.02
PM	(o)	C8n.1n	25.26	68R-2,	20	68R-2,	75	643.38	0.27
PM	(y)	C8n.2n	25.30	69R-2,	20	69R-2,	25	652.58	0.02
PM	(o)	C8n.2n	25.99	71R-6,	115	72R-1,	10	678.98	0.92
PM	(y)	C9n	26.42	73R-4,	90	75R-1,	15	701.66	7.09
PM	(o)	C9n	27.44	76R-6,	35	76R-6,	40	725.09	0.02
PM	(o)	C11n.2n	29.97	82R-6,	35	82R-6,	40	782.68	0.03
PM	(y)	C13n	33.16	93R-1,117		93R-2,	28	878.00	0.23

980

Table 3

In situ taxa	Reworked taxa
Adnatosphaeridium? sp.	Achilleodinium biformoides
Ataxodinium choane	Achomosphaera alcicornu
Batiacasphaera compta	Aiora fenestrata
Batiacasphaera spp. (pars.)	Aireiana verrucosa
Batiacasphaera hirsuta	Adnatosphaeridium spp.
Batiacasphaera micropapillata	Alisocysta circumtabulata
Batiacasphaera minuta	Alterbidinium distinctum
Batiacasphaera sphaerica	Apectodinium spp.
Batiacasphaera sp. A	Arachnodinium antarcticum
Batiacasphaera sp. B	Areoligera spp. (pars)
Batiacasphaera sp. C	Areoligera semicirculata
Batiacasphaera sp. D	Cerebrocysta bartonensis
Brigantedinium simplex	Charlesdowniea clathrata
Brigantedinium pynei	Charlesdowniea edwardsii
Brigantedinium sp. A	Cooksonidinium capricornum
Brigantedinium sp. B	Cordosphaeridium fibrospinosum
Brigantedinium sp. C	Cordosphaeridium furniculatum
Brigantedinium sp. D	Corrudinium incompositum
Cerebrocysta WR small	Corrudinium regulare
Cerebrocysta delicata	Cribroperidinium spp.
Cerebrocysta sp. A	Damassadinium crassimuratum
Cleistosphaeridium sp. B	Dapsilidinium spp.
Cleistosphaeridium sp.A	Deflandrea sp. A sensu Brinkhuis et al., 2003
Cordosphaeridium minutum	Deflandrea antarctica
Corrudinium labradori	Deflandrea cygniformis
Corrudinium sp. A	Diphyes colligerum
Cryodinium? sp.	Deflandrea spp. Indet
Distatodinium spp.	Eisenackia circumtabulata
Edwardsiella sexispinosa	Enneadocysta diktyostila
Elytrocysta sp. A	Enneadocysta multicornuta
Elytrocysta brevis	Eocladopyxis tesselata
Gelatia inflata	Fibrocysta axialis
Habibacysta? spp.	Glaphyrocysta intricta
Homotryblium spp.	Glaphyrocysta pastielsii
Hystrichokolpoma bullatum	Heteraulacacysta leptalea
Huystrichosphaeropsis obscura	Histiocysta palla
Impagidinium spp. (pars)	Hystrichokolpoma pusilla
Impagidinium aculeatum	Hystrichokolpoma rigaudiae
Impagidinium cantabrigiense	Hystrichokolpoma truncatum
Impagidinium elegans	Hystrichosphaeridium truswelliae
Impagidinium elongatum	Hystrichosphaeridium tubiferum
Impagidinium pacificum	Impagidinium maculatum
Impagidinium pallidum	Impagidinium waipawense
Impagidinium paradoxum	Kenleyia spp.
Impagidinium patulum	Manumiella druggii
Impagidinium plicatum	Melitasphaeridium pseudorecurvatum
Impagidinium velorum	Membranophoridium perforatum
Impagidinium victorianum	Octodinium askiniae
Impagidinium sp. A	Odontochitina spp.
Impagidinium sphaericum	Operculodinium spp.
Invertocysta tabulata	Phthanoperidinium antarcticum
Islandinium spp.	Phthanoperidinium echinatum
Lejeunecysta attenuata	Polysphaeridium spp.
Lejeunecysta adeliense	Rhombodinium sp.
Lejeunecysta fallax	Schematophora speciosa
Lejeunecysta cowei	Schematophora obscura
Lejeunecysta acuminata	Senegalinium spp.
Lejeunecysta rotunda	Spinidinium luciae
Lejeunecysta katatonos	Spinidinium macmurdoense
Malvinia escutiana	Spinidinium schellenbergii
Nematosphaeropsis labyrinthus	Spiniferites ramosus CPX
Oligokolpoma galeotti	Thalassiphora pelagica
Operculodinium tiara	Turbiosphaera filosa
Operculodinium sp. A	Turbiosphaera sagena
Operculodinium piaseckii	Vozzhennikovia apertura/ S.schellenbergii group
Operculodinium janduchenei	Vozzhennikovia netrona
Operculodinium cf eirikianum	?Vozzhenikovia LARGE
Operculodinium eirikianum	Wetzeliella articulata
Paleocystodinium golzowense	
Paucisphaeridium spp.	
Phthanoperidinium amoenum	
Pyxidinopsis spp. (pars)	
Pyxidinopsis sp. A	
Pyxidinopsis sp. B	
Pyxidinopsis sp. C	
Pyxidinopsis sp. D	
Pyxidinopsis vesciculata	
Pyxidinopsis tuberculata	
Pyxidinopsis reticulata	
Pyxidinopsis fairhavensis	
Reticulatosphaera actinocoronata	
Selenopemphix antarctica	
Selenopemphix nephroides	
Selenopemphix dioneacysta	
Selenopemphix sp. A	
Selenopemphix undulata	
Selenopemphix brinkhuisi	
Spiniferites sp. B	
Spiniferites sp. A	
Spiniferites sp. C	
Stoveracysta ornata	
Stoveracysta kakanuiensis	
?Svalbardella spp.	
Tectatodinium spp.	
Unipontedinium aquaeductus	
Protoperidinioid indet	
Protoperidinium sp. B	
Protoperidinium sp. A	
Protoperidinium sp. C	
Protoperidinium sp. D	

981